Formation of Solitary Waves in Collective Motion of Self-Propelled Particles

石橋, 和也

Formation of Solitary Waves in Collective Motion of Self-Propelled Particles

Kazuya Ishibashi

Contents

Chapter I

General introduction

I. INTRODUCTION

You can see the collective motion of self-propelled particles such as schools of fish, flocks of birds, herds of animals, and bacterial colonies in nature. We call them that move autonomously self-propelled particles. They include living and non-living things, such as automobiles, vibrating granular rods, and Janus particles. Vicsek and co-workers proposed a simple agent-based model for a large population of self-propelled particles to understand the collective motion in a large population [1]. Since then, it has been intensively studied [2].

A. The Vicsek model

The Vicsek model was proposed for describing the collective motion of individual living things. Self-propelled particles corresponding to living things move in two dimensions at the same speed. Since the particles are point particles, there is no exclusive interaction. The model does not consider attraction and repulsion interactions. The interaction with particles in its neighborhood determines the direction of motion of its particle in the next step. The Vicsek model has the interaction only aligning the direction of motion of the particles; it has noise interfering with the alignment. It is similar to the spin dynamics of the XY model. The Vicsek model can be thought of as an XY model in which the spins move in two-dimensional space. The Vicsek model with zero velocity of particles is analogous to the XY model.

The Vicsek model is known to have three states: the disordered state, the ordered state, and the traveling band state. In the disordered state, the self-propelled particles move in random directions, as shown in Fig. I.1(a). In the ordered state, the self-propelled particles move in concert, as shown in Fig. I.1(b). There is another collectively moving state called traveling band state (or solitary wave state), as shown in Fig. I.1(c). The solitary state appears in a narrow region between the disordered and ordered states. The solitary wave is

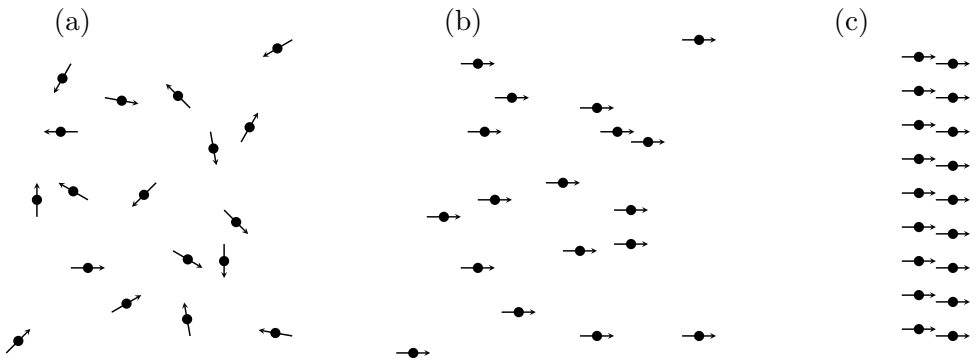

FIG. I.1: Sketch of three states in Vicsek model. The arrows indicate the direction of motion of self-propelled particles. (a) Disordered state. (b) Ordered state. (c) Solitary wave state.

a dissipative soliton, not a soliton.

Figure I.2 shows the trajectory of particles in the direction of motion [1]. The arrows indicate the direction of motion of the particles. The top left of Fig. I.2 shows the initial setup of particles in the Vicsek model. Initially, the particles move randomly. The top right of Fig. I.2 shows the trajectory after a lapse of time at low particle density and noise. The particles move in several groups. The bottom left of Fig. I.2 shows the trajectory after a lapse of time at high particle density and noise. The particles move randomly, as shown in the top left of Fig. I.2. The bottom right of Fig. I.2 shows the trajectory after a lapse of

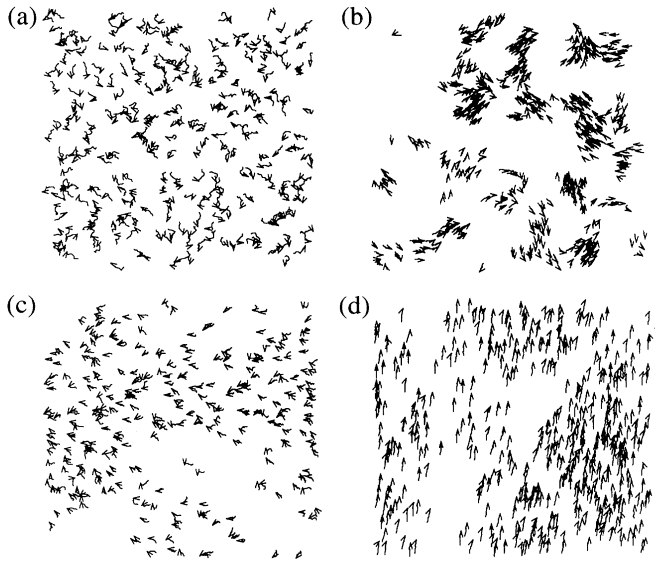

FIG. I.2: Trajectory of particles on a two-dimensional plane. Source: From Ref. [1], page 1227.

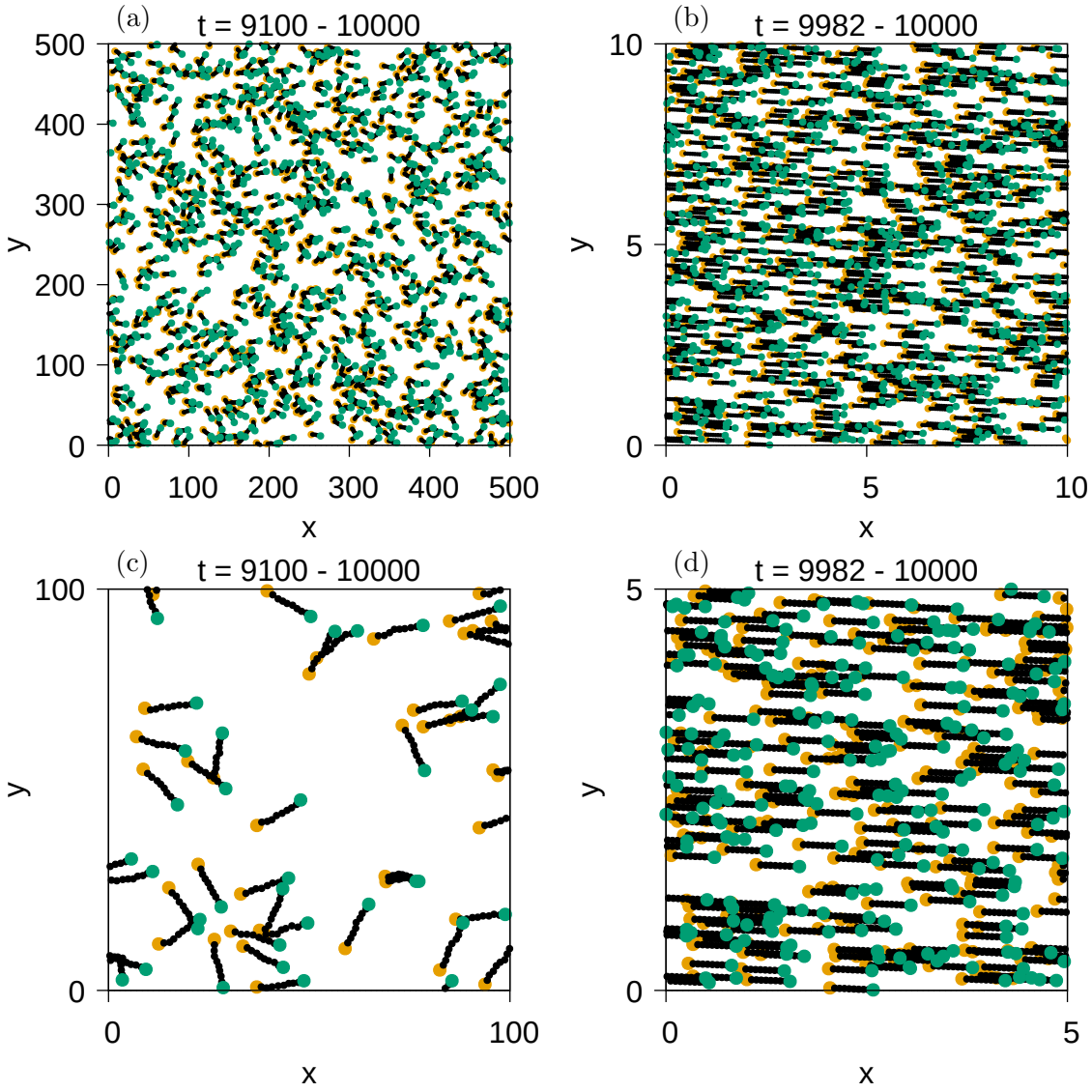

FIG. I.3: Trajectory of particles on a two-dimensional plane. The vermillion and green points indicate the first (t = 9100 or 9982) and last (t = 10000) plots. The trajectories are plotted 10 every 100 ((a) and (c)) or 2 ((b) and (d)) steps. Parameters: $N = 1000$, $v = 0.03$, $r = 1$, and $\Delta t = 1$ (a) Particles moving independently of each other. $\eta = 4$. (b) Particles moving in concert. $L_x \times L_y = 10 \times 10$, $\eta = 0.01$. (c) The enlarged view of (a). (d) The enlarged view of (b).

time at high particle density and small noise. Particles move in aligned directions. It is the ordered state.

We introduce simulation results in the Vicsek model. The original model's equation as [1]

$$\boldsymbol{x}_i(t + \Delta t) = \boldsymbol{x}_i(t) + \boldsymbol{v}_i(t)\Delta t, \tag{I.1}$$

where $\boldsymbol{x}_i(t)$ and $\boldsymbol{v}_i(t)$ the position and velocity of ith particle at time t. In this paper, we use a speed of the velocity, $v = 0.03$. Particles N are randomly set on a plane, $L_x = L_y$. Periodic boundary conditions are assumed. An angle of particles is chosen randomly as an initial condition. In the next step, the angle is determined as

$$\theta(t + \Delta t) = \langle \theta(t) \rangle_r + \Delta\theta, \tag{I.2}$$

where the first and second term of the right-hand side are average direction within radius r and a noise. The average includes itself. The average direction is as $\arctan[\langle sin(\theta(t)) \rangle_r / \langle cos(\theta(t)) \rangle_r]$. The noise is randomly chosen in the range of $-\eta/2$ to $\eta/2$. Figure I.3 shows Trajectories of particles in the Vicsek model that we performed a numerical simulation. Figure I.3(a) and I.3(c) show particles move independently of each other like random. I.3(b) and I.3(d) show particles move in concert in the right direction.

B. Collective motion

The collective state has been observed in various biological and nonbiological systems [3–7]. Besides these studies, many studies focus on the dynamics of each self-propelled particle [8]. Theoretically, phenomenological hydrodynamic equations in a large population have been investigated [9, 10]. The collective directional motion appears as a kind of order–disorder transition in a large population of self-propelled particles. In contrast to thermal equilibrium systems of short-range interactions at a finite temperature, the long-range order exists even in two dimensions. The long-range order does not appear owing to the Mermin–Wagner theorem. The transition to the collective motion is considered to be a first-order one. That is, the order parameter jumps at the transition [11].

Many self-propelling animals make a flock. That is, there are localized clusters of self-propelled units. There might be many mechanisms of clustering [12], but it was found even in the Vicsek model that localized regions of high density propagate with a constant velocity similarly to solitary waves [13]. The particles are densely packed in the black band propagating to the right in Fig. I.4. High-density band regions of the ordered state move in the background of the low-density regions. The solitary wave state appears near the transition point. This phenomenon was investigated as the instability of the spatially uniform state in hydrodynamic equations for active matters [14–16]. Ihle studied the solitary

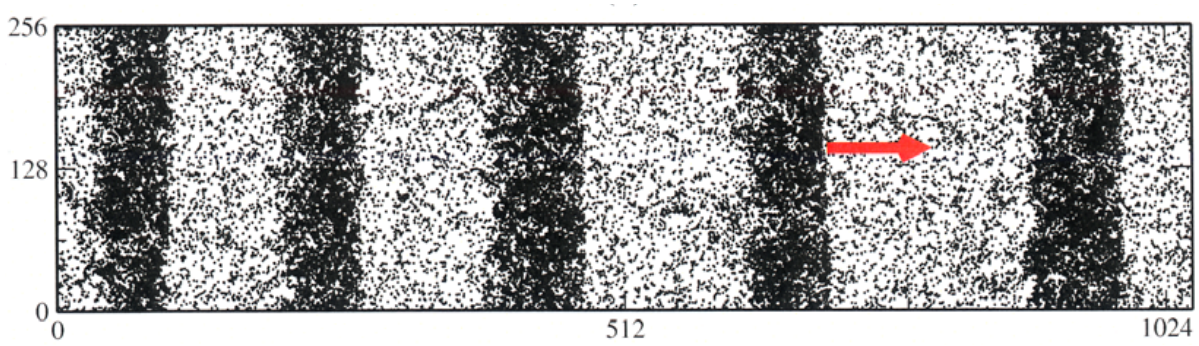

FIG. I.4: Solitary wave state. Source: From Ref. [13], page 452.

wave state by performing numerical simulations of a model system based on Enskog-like kinetic theory [17]. However, the mechanism of the formation is not fully understood. Since the hydrodynamic system is dissipative, the solitary wave is related to dissipative solitons found in many nonlinear non-equilibrium systems [18–21]. Many authors reported the solitary wave state called traveling band state in collective motion [13–17, 22–26]. The traveling band state has a quasi-one-dimensional structure; that is, the density difference appears only in the moving direction, and the density is homogeneous in the perpendicular direction. The formation mechanism of the traveling band state has been discussed by several authors [14, 25, 27, 32]. It was shown that the traveling band state appears when the spatially homogeneous ordered state is linearly unstable in the hydrodynamic description of self-propelled particles.

Figure I.5 shows the collision of the two clusters formed by the cellular slime mold. They are non-chemotactic Dictyostelium discoideum mutants. The wild-type cells in nature have chemotactic. When they are starving, they exercise randomly in search of food. When there is still no food, they aggregate to form a multicellular structure like a slug. Later, they form a fruiting body—the cells at the top fly far away in search of a good environment. The lower part is sacrificed for them. Non-chemotactic Dictyostelium discoideum mutants, which do not aggregate under starvation, form a soliton-like structure. The mutants slip through each other at a collision, so the soliton is maintained after the collision.

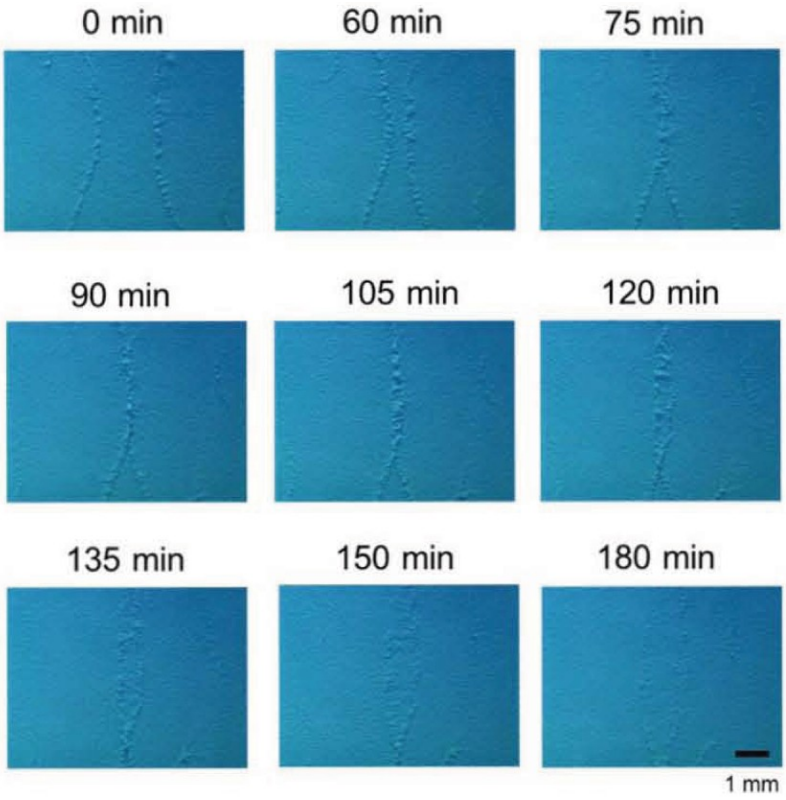

FIG. I.5: The collision of two soliton-like structures. Source: From Ref. [23], page 2.

C. The Kramers equation

The original Vicsek model has a form similar to non-locally coupled oscillators [28]. The non-locally coupled stochastic oscillators can be studied with the Fokker–Planck equation using the mean-field approximation [29, 30]. We apply the method of the nonlinear Fokker–Planck equation to the problem of self-propelled particles. Here, we think of an example when a particle, having velocity v and position x, obeys a Langevin equation in a harmonic potential [33].

$$\frac{dx}{dt} = v, \tag{I.3a}$$

$$\frac{dv}{dt} = -\alpha v - kx + \xi(t), \tag{I.3b}$$

where α and k are coefficients, the second term is a external force and the third term in Eq. (I.3b) is a noise. Using the Kramers–Moyal expansion to Eq. I.3, we derive a partial differential equation describing the time variation of the probability density. The Kramers–

Moyal expansion is described as

$$\frac{\partial P}{\partial t} = \sum_{n=1}^{\infty} \frac{(-1)^n}{n!} \frac{\partial^n}{\partial x^n} \left[\alpha_n(x) P(x,t|x_0) \right], \tag{I.4}$$

where α_n is defined as

$$\lim_{\Delta t \to 0} \frac{1}{\Delta t} \int_{-\infty}^{\infty} (\Delta x)^n P(x + \Delta x, \Delta t|x) d\Delta x = \lim_{\Delta t \to 0} \frac{\langle (\Delta x)^n \rangle}{\Delta t}. \tag{I.5}$$

If the change of the external force kx relative to the space is smooth, the changes in Eq. (I.3) between t and $t + \Delta t$ are

$$x(t + \Delta t) - x(t) = \int_t^{t+\Delta t} v(t') dt' = v(t) \Delta t, \tag{I.6a}$$

$$v(t + \Delta t) - v(t) = -(\alpha v + kx)\Delta t + \int_t^{t+\Delta t} \xi(t') e^{-\gamma(t-t')} dt'. \tag{I.6b}$$

The equations calculated to the second moment of x and v are

$$\lim_{\Delta t \to 0} \frac{\langle x(t + \Delta t) - x(t) \rangle}{\Delta t} = v, \tag{I.7a}$$

$$\lim_{\Delta t \to 0} \frac{\langle v(t + \Delta t) - v(t) \rangle}{\Delta t} = -(\alpha v + kx), \tag{I.7b}$$

$$\lim_{\Delta t \to 0} \frac{\langle (v(t + \Delta t) - v(t))^2 \rangle}{\Delta t} = 2\alpha k_B T. \tag{I.7c}$$

The corresponding Kramers equation is expressed as

$$\frac{\partial P(x,v,t)}{\partial t} = \left[-\frac{\partial}{\partial x} v + \frac{\partial}{\partial v} (\alpha v + kx) + \alpha k_B T \frac{\partial^2}{\partial v^2} \right] P(x,v,t). \tag{I.8}$$

This equation has two independent variables, x and v, besides time t. If the equation has only one independent variable, It is called the Fokker–Planck equation.

The dynamics of the probability distributions for the velocity and position of self-propelled particles are studied using the nonlinear Kramers equation. We show that a solitary wave state appears owing to instability from a spatially uniform ordered state in the nonlinear Kramers equation. The solitary wave state is a non-equilibrium state; the non-equilibrium phase transition of self-propelled particles generates it. The non-equilibrium phase transition can be clearly seen because the probability distributions are directly obtained in the numerical simulation of the nonlinear Kramers equation. First, we show that the solitary wave state appears in the one-dimensional nonlinear Kramers equation; it is a time evolution equation of the probability distribution for the position x and velocity v_x of

self-propelled particles [31]. However, there are three important variables, the direction of the velocity and the x, y coordinates, in the original two-dimensional Vicsek model. The magnitude of the velocity is fixed to be a constant. We consider introducing the momentum direction so that the direction in the one-dimensional model can correspond to the direction in two dimensions similar to the Vicsek model. The angle ϕ from the x-axis expresses the momentum direction. Next, we show the solitary wave state in the one-dimensional nonlinear Kramers equation for the angle ϕ and the position x [32].

D. Ising-type Vicsek model

In the original two-dimensional Vicsek model, self-propelled particles can move in any direction, and the particles move simultaneously in the next step. Solon and Tailleur proposed the active Ising model (AIM), in which particles hop to the left or right lattice point stochastically. In the AIM, multiple particles can stay at one lattice site [34]. In one dimension, there are two kinds of state: a disordered state and flipping cluster state, and there is no ordered state owing to strong fluctuations [34–36]. In the flipping cluster state, a moving cluster of high density appears in the background of a low-density region; however, the moving direction is not constant and changes stochastically. In two dimensions, there are three kinds of state: disordered and ordered states and a traveling band state. In the traveling band state, a high-density band appears in the background of the low-density region, and it moves in a certain direction with a steady velocity. The number of high-density bands is one in the AIM, although there are multiple bands in the traveling band state of the Vicsek model. The traveling band state is interpreted to be generated from the motility-induced phase separation in active matter [37, 38]. When self-propelled particles are concentrated, the particles slow down due to the crowding, and the concentration of particles increases further. The positive feedback induces phase separation. The attractive force among particles is not necessary for this phase separation mechanism. Later, the active Potts model (APM) was proposed in two dimensions in analogy with the active Ising model to take in more possibilities of moving directions, i.e., right, left, up, or down on a square lattice. A high-density band appears in the background of the low-density region also in the APM. It was found that the direction of collective motion of particles changes with the control parameter in the APM [39, 40]. No flipping motions were observed in AIM or APM in two

dimensions.

We are interested in the flipping cluster state in the one-dimensional AIM. In this state, a cluster of self-propelled particles changes its moving direction in a stochastic manner. Solon and Tailleur did not study this state in detail, probably because this state did not appear in two dimensions. In nature, stochastic changes in the moving direction of clusters are often observed in flocks of birds such as starlings. The collective behavior of starling flocks was studied by direct measurement [41]. On the other hand, complicated motions, including reciprocal motions of a single active particle, were studied by many authors [42–44]. However, the flipping motions of clusters were not studied in detail. We proposed a modified model of AIM to understand the flipping cluster state [45]. The self-propelled particles move on a one-directional lattice with velocity ± 1, which is similar to the AIM. We assumed that the moving direction of a particle on a lattice site is determined by a majority rule among the self-propelled particles on the lattice site and its nearest-neighbor sites. We call this model Ising-type Vicsek model. The probability of the moving direction is determined by the interaction with particles in the surrounding sites, and the update of position and velocity of each particle is performed simultaneously for all particles. In our model, flip motions of a cluster of particles occur very sharply in contrast to those in the one-dimensional AIM. We show that the sweeping-up process occurs with the rapid change in the moving direction, and fluctuation is essentially important for the nucleation of a seed of a cluster of inversely moving particles. Next, we propose Potts-type Vicsek models and show that the flipping cluster state appears even in two dimensions, which was not observed in the AIM or APM.

Chapter Ⅱ

Solitary wave states in the nonlinear Kramers equation

I. ONE-DIMENSIONAL NONLINEAR KRAMERS EQUATION WITH VELOCITY AS A VARIABLE

The original Vicsek model has a form similar to non-locally coupled oscillators [28]. The non-locally coupled stochastic oscillators can be studied with the Fokker–Planck equation using the mean-field approximation [29, 30]. Here, we apply the method of the nonlinear Fokker–Planck equation to the problem of self-propelled particles. We consider a large population of non-locally coupled self-propelled particles in one dimension for the sake of simplicity. The model equation is expressed with the Langevin equation

$$\frac{dx_i}{dt} = v_i, \tag{II.9a}$$

$$\frac{dv_i}{dt} = \mu v_i - v_i^3 + g\sum_{j=1}^{N} e^{-\alpha\{1-\cos(2\pi(x_j-x_i)/L)\}}(v_j - v_i) + \xi_i(t), \tag{II.9b}$$

where x_i and v_i are the x coordinate and velocity of the ith element. L is the system size. $\xi_i(t)$ is Gaussian white noise satisfying $\langle \xi_i(t)\xi_j(t')\rangle = 2T\delta_{i,j}\delta(t-t')$. If $g = T = 0$, each elemental particle becomes a self-propelled particle of velocity $v = \pm\sqrt{\mu}$ for $\mu > 0$. The nonlocal interaction in the spatially periodic one-dimensional system of size L is expressed by the third summation term on the right-hand side of Eq. (II.9b). The nonlocal interaction tends to make the velocities of active particles uniform. Similar terms to align the velocities are assumed in the Vicsek model and many other related models. However, our model is simpler than those models in that it is a one-dimensional model in contrast to the Vicsek type models in two dimensions. The integral kernel $e^{-\alpha\{1-\cos(2\pi(x'-x)/L)\}}$ is approximated by the Gaussian function $e^{-(2\pi^2\alpha/L^2)(x'-x)^2}$ if $x'-x$ is sufficiently small. For example, the Gaussian approximation is good for $\alpha = 10$ and $L = 5$, which are typical parameter values used in later numerical simulations. We chose the integral kernel because the relatively

simple function is well approximated locally by the Gaussian and has a spatial periodicity of period L.

The Kramers equation corresponding to the Langevin equation of Eq. (II.9) is expressed as

$$\frac{\partial P}{\partial t} = -\frac{\partial}{\partial x}(vP) - \frac{\partial}{\partial v}\left[\left\{\mu v - v^3 + g\int_0^L e^{-\alpha\{1-\cos(2\pi(x'-x)/L)\}}\rho(x')(u(x')-v)dx'\right\}P\right] + T\frac{\partial^2 P}{\partial v^2}, \tag{II.10}$$

where $P(x,v,t)$ is the probability density function, $\rho(x) = \int_{-\infty}^{\infty} P(x,v,t)dv$ denotes the density at position x, and $u(x) = \int_{-\infty}^{\infty} vP(x,v,t)dv/\rho(x)$ denotes the average velocity at the position. If each particle interacts non-locally with a sufficiently large number of particles, a mean-field approximation can be applied even in one dimension [29, 30]. In our model of non-locally coupled active particles, we assume a kind of mean-field approximation by replacing the summation in Eq. (II.9b) with the integral expressed in terms of the density $\rho(x)$ and average velocity $u(x)$. The Kramers equation is a deterministic equation for non-locally coupled self-propelled particles, and thus phase transitions can be treated as bifurcations in the nonlinear equation. The Kramers equation is a nonlinear equation, because $\rho(x)$ and $u(x)$ in the second term on the right-hand side of Eq. (II.10) are determined by $P(x,v,t)$. Furthermore, the normalization condition $\int_0^L \int_{-\infty}^{\infty} P(x,v,t)dvdx = 1$ is assumed in this paper.

If the system is spatially uniform, $\partial P/\partial x = 0$ and $\rho(x) = 1/L$. Then, Eq. (II.10) is reduced to

$$\frac{\partial P}{\partial t} = -\frac{\partial}{\partial v}\left[\left\{\mu v - v^3 + \frac{g}{L}\int_0^L e^{-\alpha\{1-\cos(2\pi(x'-x)/L)\}}(u(x')-v)dx'\right\}P\right] + T\frac{\partial^2 P}{\partial v^2}. \tag{II.11}$$

The free energy density F/L is defined as

$$F/L = \int_{-\infty}^{\infty}\left[\left\{-(1/2)\mu v^2 + (1/4)v^4 + \frac{g}{L}\int_0^L e^{-\alpha\{1-\cos(2\pi(x'-x)/L)\}}(-u(x')v + (1/2)v^2)dx'\right\}P\right]dv + T\int_{-\infty}^{\infty} P\log P dv. \tag{II.12}$$

The free energy decreases in the time evolution of Eq. (II.11), that is, F is the Lyapunov function of Eq. (II.11).

The equilibrium probability distribution is given by

$$P_{eq}(v) = ce^{[(1/2)\mu v^2 - (1/4)v^4 - r\{-uv + (1/2)v^2\}]/T}, \tag{II.13}$$

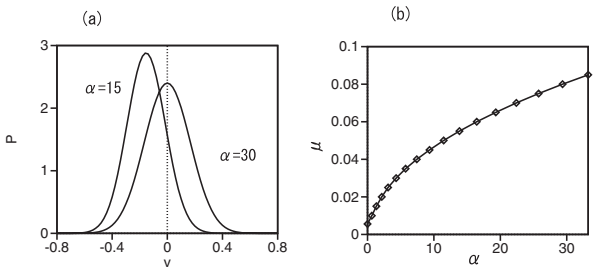

FIG. II.1: (a) Equilibrium distributions at $\alpha = 15$ and 30 for $\mu = 0.08$, $T = 0.1$, $g = 50$, and $L = 5$. (b) Critical line in the parameter space (α, μ) for $\mu = 0.08$, $T = 0.1$, $g = 50$, and $L = 5$.

where $r = g/L \int_0^L e^{-\alpha\{1-\cos(2\pi(x'-x)/L)\}} dx$ and $c = 1/\int_{-\infty}^{\infty} P_{eq}(v)dv$ is the normalization constant. The spatially uniform average velocity u satisfies

$$u = \int_{-\infty}^{\infty} P_{eq}(v) v dv, \tag{II.14}$$

where P_{eq} includes u and therefore Eq. (II.14) is a self-consistent equation. The average velocity u is a solution to this self-consistent equation. If the Taylor series expansion is applied to the right-hand side of Eq. (II.14) with respect to u, only the odd-power terms of u appear, that is, the Taylor expansion is expressed as $c_1 u + c_3 u^3 + c_5 u^5 + \cdots$, because the function $e^{[(1/2)\mu v^2 - (1/4)v^4 - (1/2)rv^2]/T}$ in $P_{eq}(v)$ is an even function of v and e^{ruv} is expanded as $1 + ruv + (1/2)(ruv)^2 + \cdots$. A pitchfork bifurcation can occur at a certain parameter value.

Figure II.1(a) shows equilibrium distributions $P_{eq}(v)$ at $\alpha = 15$ and 30 for $\mu = 0.08$, $T = 0.1$, $g = 50$, and $L = 5$. The average value u can be obtained by solving the self-consistent equations Eqs. (II.13) and (II.14) with the iteration method. The average velocity u is 0 at $\alpha = 30$ and takes a nonzero value at $\alpha = 15$ as a result of the symmetry-breaking phase transition. In Fig. II.1(a), the average value u is negative but it can take a positive value owing to the symmetry. There is an order–disorder phase transition at $\alpha \simeq 29.4$. This transition is a second-order phase transition, and the absolute value of the average velocity increases continuously from 0. The first coefficient c_1 of the Taylor expansion becomes 1 at the phase transition. This condition is explicitly expressed as

$$\frac{\int_{-\infty}^{\infty} (r/T) v^2 e^{(\mu/2)v^2 - (1/4)v^4/4 - (r/2)v^2} dv}{\int_{-\infty}^{\infty} e^{(\mu/2)v^2 - (1/4)v^4/4 - (r/2)v^2} dv} = 1. \tag{II.15}$$

Figure II.1(b) shows the numerically obtained critical line satisfying Eq. (II.15) in the parameter space (α, μ). For $\mu > 0$, each particle is a self-propelled particle, but collective

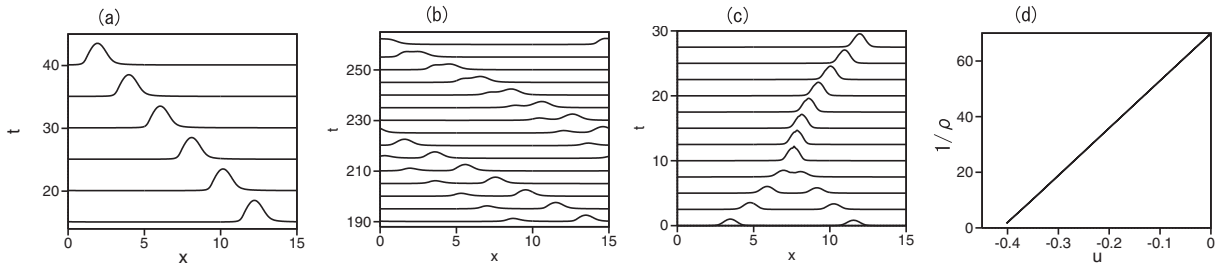

FIG. II.2: (a) Traveling solitary wave state at $\mu = 0.2$, $\alpha = 180$, $T = 0.1$, $g = 50$, and $L = 15$. (b) Merging process of two solitary waves at $\mu = 0.2$, $\alpha = 180$, $T = 0.1$, $g = 50$, and $L = 15$. (c) Head-on collision of two solitary waves at $\mu = 0.2$, $\alpha = 180$, $T = 0.1$, $g = 50$, and $L = 15$. (d) Relationship between the average velocity $u(x)$ and $1/\rho(x)$.

motion appears above the critical line owing to the effect of noises.

II. SOLITARY WAVE STATE IN THE NONLINEAR KRAMERS EQUATION WITH VELOCITY AS A VARIABLE

The spatially uniform state is not always stable. A solitary traveling wave appears when the spatially uniform self-driving state becomes unstable. We performed a direct numerical simulation of Eq. (II.10) with the simple Euler method of time-step $\Delta t = 0.0005$. The coordinate x and velocity v are respectively discretized by $\Delta x = 1/40$ and $\Delta v = 1/50$.

Figure II.2(a) shows the time evolution of $\rho(x,t) = \int_{-\infty}^{\infty} P(x,v,t)dv$ for $\mu = 0.2$, $\alpha = 180$, $T = 0.1$, $g = 50$, and $L = 15$. The solitary wave propagates with a constant velocity $v_0 \simeq -0.4116$. The peak density is $\rho(x) \simeq 0.588$ and the density takes a small value of $\rho(x) \simeq 0.0144$ in the region distant from the peak position. A pulse train state at a final stationary state did not also appear under other initial conditions. Figure II.2(b) shows the time evolution from an initial condition with two peaks of $\rho(x)$ for the same parameter values as in Fig. II.2(a). The solitary wave with the higher peak moves faster than, the lower peak. The higher solitary wave catches up with the lower one, and the two solitary waves merge into an even higher solitary wave. Figure II.2(c) shows the time evolution of the head-on collision of two solitary waves moving in opposite directions with slightly different amplitudes at the same parameters as in Fig. II.2(a). The two solitary waves merge, and one solitary wave traveling in the right direction arises, which is the direction of the solitary wave with a

larger amplitude. Generally, various phenomena such as pair annihilation, interpenetration, and the formation of a bound state occur at the head-on collision of two dissipative solitons, depending on the control parameters [20, 21]. The merging in our system corresponds to forming a bound state, which is one of the typical behaviors. Ihle found the interpenetration of two solitary waves at multiple head-on collisions in a numerical simulation of the model based on kinetic theory. However, the amplitude difference between the two solitary waves increases at each collision, and finally, only one solitary wave survives.

Figure II.2(d) shows the relation between $u(x)$ and $1/\rho(x)$ for the final state in Fig. II.2(a). The average velocity $u(x)$ becomes 0 in the lowest-density region of $\rho \simeq 0.0144$, because the disordered state appears when $\rho < \rho_c = 0.062$ in the spatially uniform state. Figure II.2(d) shows clearly that $\rho(x,t)$ and $u(x,t)$ satisfy $\rho(x) \propto 1/(u(x) - v_0)$. This nontrivial relation is derived as follows. The integration of Eq. (II.10) with respect to v yields

$$\frac{\partial \rho}{\partial t} = -\frac{\partial}{\partial x}(u\rho), \tag{II.16}$$

if $P(x,v,t) \to 0$ and $\partial P/\partial v \to 0$ are satisfied for $v \to \pm\infty$. If the wave propagates with a constant velocity v_0, then $\partial\rho/\partial t = -v_0 \partial\rho/\partial x$, therefore,

$$\frac{\partial}{\partial x}\left\{(u(x) - v_0)\rho\right\} = 0. \tag{II.17}$$

Thus, the relation $\rho(x,t) \propto 1/(u(x) - v_0)$ is satisfied.

The explicit form of the solitary wave is not yet known. We assume an approximate solution of the form $P(x,v,t) = \rho(x - v_0 t) f(v,t)$ to understand the solitary wave state qualitatively. That is, $P(x,v,t)$ is expressed as the product of the propagating density and the probability distribution of v under the nonuniform density $\rho(x - v_0 t)$. As an approximation, the probability distribution f of v satisfies the Fokker–Planck equation:

$$\frac{\partial f}{\partial t} = -\frac{\partial}{\partial v}\left[\left\{\mu v - v^3 + g\int_0^L e^{-\alpha\{1-\cos(2\pi(x'-x)/L)\}}\rho(x')(u(x') - v)dx'\right\} f\right] + T\frac{\partial^2 f}{\partial v^2}. \tag{II.18}$$

The equilibrium distribution f is given by

$$f_{eq}(x,v) \propto e^{\{(1/2)\mu v^2 - (1/4)v^4 + Av - (1/2)Bv^2)\}/T}, \tag{II.19}$$

where

$$A(x) = g\int_0^L e^{\alpha\{1-\cos(2\pi(x'-x)/L)\}}\rho(x')u(x')dx',\ B(x) = g\int_0^L e^{\alpha\{1-\cos(2\pi(x'-x)/L)\}}\rho(x')dx'.$$

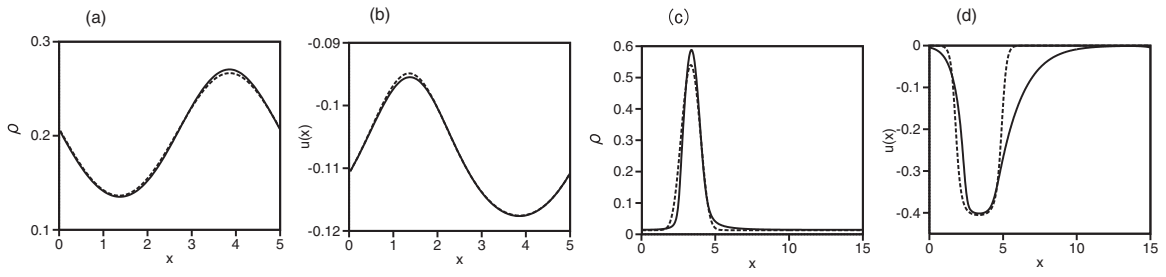

FIG. II.3: (a) Comparison of the density $\rho(x)$ (solid line) obtained by direct numerical simulation and $\rho(x)$ (dashed line) obtained by the self-consistent method for $\mu = 0.07$, $\alpha = 16$, $T = 0.1$, $g = 50$, and $L = 5$. (b) Comparison of the average velocity $u(x)$ (solid line) obtained by direct numerical simulation and the average velocity $u(x)$ (dashed line) obtained by the self-consistent method for the same parameters as in (a). (c) Comparison of the densities $\rho(x)$ obtained by the two methods for $\mu = 0.2$, $\alpha = 180$, $T = 0.1$, $g = 50$, and $L = 15$. (d) Comparison of the average velocities $u(x)$ obtained by the two methods for the same parameters as in (c).

$A(x)$ and $B(x)$ are spatially dependent mean fields which determine the velocity distribution of self-propelled particles. The average velocity $u(x)$ is given by $u(x) = \int_{-\infty}^{\infty} v f_{eq}(v) dv$. The spatially dependent average velocity $u(x)$ is determined self-consistently because $A(x)$ in $f_{eq}(v)$ is calculated using $u(x)$. The quantity $u(x)$ is numerically obtained by iterating the integrals $A(x) = g \int_0^L e^{\alpha\{1-\cos(2\pi(x'-x)/L)\}} \rho(x') u(x') dx'$ and $u(x) = \int_{-\infty}^{\infty} v f_{eq}(v) dv$. If the average velocity $u(x)$ is obtained, the average density $\rho(x)$ is evaluated as $\rho(x) \propto 1/|u(x) - v_0|$. We attempted to obtain the solutions of $\rho(x)$, $u(x)$, $A(x)$, and $B(x)$ by this iteration method for several values of $v_0 (< 0)$. We found that $\rho(x)$ increases to infinity for $v_0 > v_{0c}$ and $\rho(x)$ decreases to 0 for $v_0 < v_{0c}$. There is a critical value of v_{0c} at which self-consistent solutions $\rho(x)$ and $u(x)$ are obtained.

Figure II.3(a) shows the density $\rho(x)$ (solid line) obtained by direct numerical simulation and $\rho(x)$ (dashed line) obtained by the self-consistent method at $v_0 = -0.14127$ for $\mu = 0.07$, $\alpha = 16$, $T = 0.1$, $g = 50$, and $L = 5$. Figure II.3(b) compares the average velocity $u(x)$ (solid line) obtained by direct numerical simulation with $u(x)$ (dashed line) obtained by the self-consistent method. The parameters are close to the instability point of the spatially uniform state, and a sinusoidal wave appears. Reasonably good agreement is seen between the numerical results and the results obtained by the self-consistent method. The critical

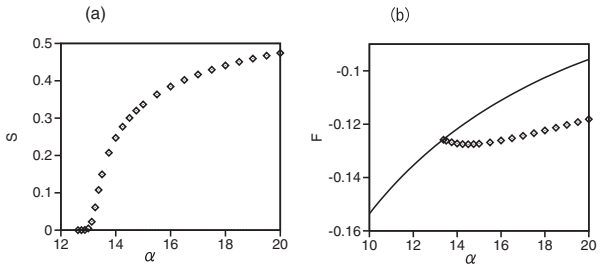

FIG. II.4: (a) Fourier amplitude S as a function of α for $\mu = 0.08$, $T = 0.1$, $g = 50$, and $L = 5$. (b) Free energy F as a function of α for $\mu = 0.08$. The solid line corresponds to the spatially uniform state and the rhombi denote the solitary wave states obtained by direct numerical simulation of Eq. (II.10).

velocity $v_{0c} = -0.14127$ is also close to the propagating velocity $v_0 = -0.1397$ of the solitary wave in the direct numerical simulation. Figures II.3(c) and 3(d) show the densities $\rho(x)$ and average velocities $u(x)$ obtained by the direct numerical simulation and the self-consistent method at $v_0 = -0.4154$ for $\mu = 0.2$, $\alpha = 180$, $T = 0.1$, $g = 50$, and $L = 15$. These parameters correspond to those used in Fig. II.2. A solitary wave state is obtained by the self-consistent method. The numerically obtained velocity $v_0 = -0.4116$ of the solitary wave is close to the critical value $v_{0c} = -0.4154$. However, some disagreement is seen, probably because the solitary wave state appears far from the instability point, where the approximation $P(x, v, t) = \rho(x - v_0 t) f_{eq}(v)$ becomes less accurate.

Phase transitions occur in the nonlinear Kramers equation when the parameters are changed. To characterize the solitary wave state, we use the Fourier amplitude S of wavenumber $2\pi/L$ defined as

$$S = \left[\left\{ \int_0^L \int_{-\infty}^{\infty} P(x,v) \sin(2\pi x/L) dv dx \right\}^2 + \left\{ \int_0^L \int_{-\infty}^{\infty} P(x,v) \cos(2\pi x/L) dv dx \right\}^2 \right]^{1/2}.$$

Figure II.4(a) shows S as a function of α for $\mu = 0.08$, $T = 0.1$, $g = 50$, and $L = 5$. S increases continuously from 0 at $\alpha \simeq 13$. The transition from the spatially uniform ordered state to the solitary wave state is a continuous transition. Figure II.4(b) shows F defined

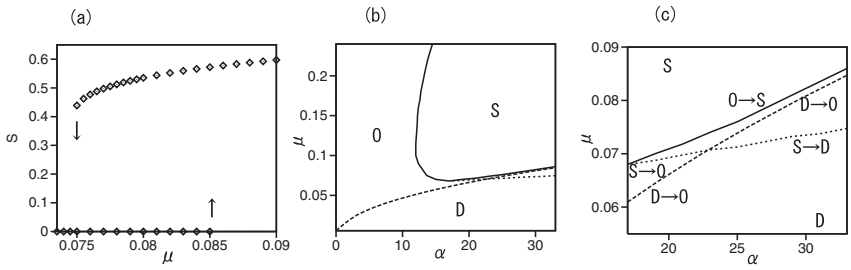

FIG. II.5: (a) Fourier amplitude S as a function of μ for $\alpha = 33$, $T = 0.1$, $g = 50$, and $L = 5$. (b) Phase diagram in the parameter space (α, μ) for $g = 50$ and $L = 5$. 'S': solitary wave state, 'D': disordered state, and 'O': spatially uniform ordered state. (c) Magnification of (b). The transition lines $S \to D$, $D \to 0$, $0 \to S$, and $S \to 0$ are shown.

by

$$F = \int_0^L \int_{-\infty}^{\infty} \left[\left\{ -\frac{\mu v^2}{2} + \frac{v^4}{4} + g \int_0^L e^{-\alpha\{1-\cos(2\pi(x'-x)/L)\}} \rho(x')(-u(x')v + v^2/2)dx' \right\} P \right] dvdx$$
$$+T \int_0^L \int_{-\infty}^{\infty} P \log P dvdx. \tag{II.20}$$

F is a simple extension of the free energy given by Eq. (II.12) for the spatially uniform state to the spatially nonuniform state. We consider F as the free energy for Eq. (II.10) in this paper, although F is not exactly the Lyapunov function of Eq. (II.10). (It is generally difficult to find the Lyapunov function in a non-equilibrium system.) The solid line denotes F for the spatially uniform state obtained using Eqs. (II.13) and (II.14). The rhombi denote F for the solitary wave state obtained by the direct numerical simulation of Eq. (II.10). The solitary wave state has lower free energy F than the spatially uniform state owing to the lower energy in the first term of Eq. (II.20). It is interesting that the self-propelled particles gather together, even if mutual attraction is not assumed.

Figure II.5(a) shows S as a function of μ for $\alpha = 33$, $T = 0.1$, $g = 50$, and $L = 5$. The solitary wave state jumps to the disordered state for $\mu < 0.0745$. The disordered state changes into the spatially ordered state at $\mu = 0.0835$, and the spatially ordered state jumps to the solitary wave state at $\mu = 0.086$. There is a small bistable region of the disordered and solitary wave states. Figure II.5(b) shows a phase diagram in the parameter space (α, μ) for $g = 50$ and $L = 5$. The solid line shows the instability line of the spatially uniform ordered state. The dashed line is the phase transition line from the disordered state to the spatially

uniform ordered state shown in Fig. II.1. The dotted line denotes the transition line from the solitary wave state to the spatially uniform states. Figure II.5(c) is a magnification of Fig. II.5(b) around the parameter region where the three lines cross. The transition between the spatially uniform states and the solitary wave state is a first-order transition for $\alpha > 17$. That is, when μ is increased from a sufficiently small value for $\alpha > 17$, the disordered state 'D' changes into the ordered state 'O' at the transition line D$\rightarrow$ O in Fig. II.5(c) and then the ordered state 'O' changes into the solitary wave state at O$\rightarrow$ S. On the other hand, when μ is decreased from a sufficiently large value, the solitary wave state changes into the disordered state at the line S$\rightarrow$ D for $\alpha > 23$ and the solitary wave state changes into the ordered state at the line S$\rightarrow$ O for $17 < \alpha < 23$. The transition, however, becomes second-order for $\alpha < 17$. That is, the disordered state changes into the ordered state, and the ordered state continuously changes into the solitary wave state as shown in Fig. II.4(a).

III. ONE-DIMENSIONAL NONLINEAR KRAMERS EQUATION WITH MOVEMENT DIRECTION AS A VARIABLE

This Chapter in Section I showed that the solitary wave state appears in the one-dimensional nonlinear Kramers equation. The nonlinear Kramers equation is a time evolution equation of the probability distribution for the position and velocity of self-propelled particles. We considered the probability distribution of the velocity v_x and position x. However, there are two important variables, the direction of the velocity and the coordinates, in the original two-dimensional Vicsek model. The magnitude of the velocity is fixed to be a constant. The momentum direction is expressed by the angle ϕ from the x-axis. This section studies the nonlinear Kramers equation for the angle ϕ and the position x.

The model equations for elemental particles are expressed by the Langevin equation

$$\frac{dx_i}{dt} = \cos\phi_i, \tag{II.21a}$$

$$\frac{d\phi_i}{dt} = g\sum_{j=1}^{N} e^{-\alpha\{1-\cos(2\pi(x_j-x_i)/L)\}}\sin(\phi_j-\phi_i) + \xi_i(t), \tag{II.21b}$$

where x_i, and ϕ_i are the position x and the angle of the movement of the ith element, respectively, L denotes the system size, and $\xi_i(t)$ is Gaussian white noise satisfying $\langle\xi_i(t)\xi_j(t')\rangle = 2T\delta_{i,j}\delta(t-t')$. In two dimensions, the magnitude of the velocity vector is

fixed to 1. In this one-dimensional model, the velocity v_x of each self-propelled particle is expressed as $\cos\phi$. At $g = 0$, each elemental particle moves independently in the direction of ϕ_i. The nonlocal interaction in the spatially periodic one-dimensional system of size L is expressed by the first term in the summation on the right-hand side of Eq. (II.21b). For $g > 0$, the direction of motion tends to be mutually aligned. The last noise term in Eq. (II.21b) makes the direction of motion random. A phase transition is expected to occur due to the competition of the two effects.

The Kramers equation corresponding to the Langevin equation is expressed as

$$\begin{aligned}\frac{\partial P}{\partial t} &= -\frac{\partial}{\partial x}\left(\cos\phi P\right) + T\frac{\partial^2 P}{\partial \phi^2} \\ &-\frac{\partial}{\partial \phi}\left[\left\{g\int_0^L e^{-\alpha\{1-\cos(2\pi(x'-x)/L)\}} r(x')\sin(\bar{\phi}(x')-\phi)dx'\right\}P\right],\end{aligned} \tag{II.22}$$

where $P(x,\phi,t)$ is the probability density function and $r(x)e^{i\bar{\phi}(x)} = \int_0^{2\pi} P(x,\phi)e^{i\phi}d\phi$. Here, we have assumed a kind of mean-field approximation in that the summation is replaced by the integral using the density and the average direction $\bar{\phi}$. This is an approximation in that some fluctuation effects and correlation effects between the direction of motion and the density are neglected. The Kramers equation is a nonlinear equation because $r(x)e^{i\bar{\phi}}$ in the third term of the right-hand side of Eq. (II.22) is expressed with the average of $e^{i\phi}$ with respect to $P(x,\phi,t)$. Since the nonlinear Kramers equation is a deterministic equation, the phase transitions can be treated as bifurcations in the nonlinear equation. In this paper, we assume the normalization condition $\int_0^L\int_0^{2\pi} P(x,\phi)d\phi dx = 1$. There is a uniform solution: $P(x,\phi) = 1/(2\pi L)$. In this uniform state, the average velocity $\langle\cos\phi\rangle$ is 0. However, for sufficiently large g, the uniform state becomes unstable, and the average velocity $\langle\cos\phi\rangle$ becomes nonzero.

If a stationary solution $P_0(x,\phi)$ does not depend on x, $P_0(\phi)$ is expressed by the thermal equilibrium distribution as

$$P_0(\phi) \propto e^{K\langle\cos\phi\rangle\cos\phi/T}, \tag{II.23}$$

where $K = (g/L_x)\int_0^{L_x} e^{-\alpha\{1-\cos(2\pi x/L)\}}dx$.

Because $\langle\cos\phi\rangle = \int_0^{2\pi} P_0(\phi)\cos\phi d\phi / \int_0^{2\pi} P_0(\phi)d\phi$, $\langle\cos\phi\rangle$ is expressed as

$$\langle\cos\phi\rangle = \frac{\int_0^{2\pi} e^{K\langle\cos\phi\rangle\cos\phi/T}\cos\phi d\phi}{\int_0^{2\pi} e^{K\langle\cos\phi\rangle\cos\phi/T}d\phi}. \tag{II.24}$$

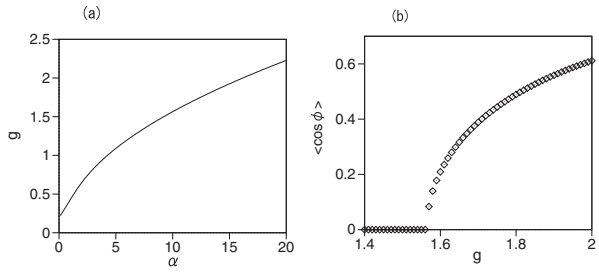

FIG. II.6: (a) Critical line in the parameter space of (α, g) at $T = 0.1$. (b) Average velocity $\langle \cos\phi \rangle$ as a function of g at $T = 0.1$.

This is a self-consistent equation for $\langle \cos\phi \rangle$. If $\langle \cos\phi \rangle$ is sufficiently small, the self-consistent equation can be approximated as

$$\langle \cos\phi \rangle \simeq \frac{\int_0^{2\pi} K \langle \cos\phi \rangle \cos^2\phi d\phi / T}{2\pi} = \frac{K}{2T} \langle \cos\phi \rangle + O(\langle \cos\phi \rangle)^3). \tag{II.25}$$

The nonzero $\langle \cos\phi \rangle$ appears for $K > K_c = 2T$. That is, the critical value of g is

$$g = \frac{2TL_x}{\int_0^{L_x} e^{-\alpha\{1-\cos(2\pi x/L_x)\}} dx} = \frac{4\pi T}{\int_0^{2\pi} e^{-\alpha(1-\cos\phi)} d\phi}. \tag{II.26}$$

The critical line does not depend on the system size L_x. Figure II.6(a) shows the critical line of Eq. (II.26) in the parameter space of (α, g) at $T = 0.1$. A nonzero $\langle \cos\phi \rangle$ appears above the critical line. Figure II.6(b) shows the average velocity $\langle \cos\phi \rangle$ as a function of g for $L_x = 10$ and $\alpha = 10$. The average velocity increases continuously from 0.

IV. SOLITARY WAVE STATE IN THE NONLINEAR KRAMERS EQUATION WITH MOVEMENT DIRECTION AS A VARIABLE

For larger g, the spatially uniform state can be unstable and a solitary wave state appears. Figure II.7(a) shows the time evolution of the density $\rho(x,t) = \int_0^{2\pi} P(x,\phi) d\phi$ at $L_x = 10$, $g = 1.44$, and $\alpha = 5$. A solitary wave propagates in the x-direction. The spatial inhomogeneity can be evaluated by the Fourier amplitude of the local order parameter

$$A = \left| \frac{1}{L_x} \int_0^L \langle \cos\phi(x) \rangle e^{i2\pi x/L} dx \right|, \tag{II.27}$$

where $\langle \cos(\phi(x)) \rangle = \int_0^{2\pi} P(x,\phi) \cos\phi d\phi / \int_0^{2\pi} P(x,\phi) d\phi$. Figure II.7(b) shows the Fourier amplitude A as a function of g for $L_x = 10$, $\alpha = 5$, and $T = 0.1$. The Fourier amplitude

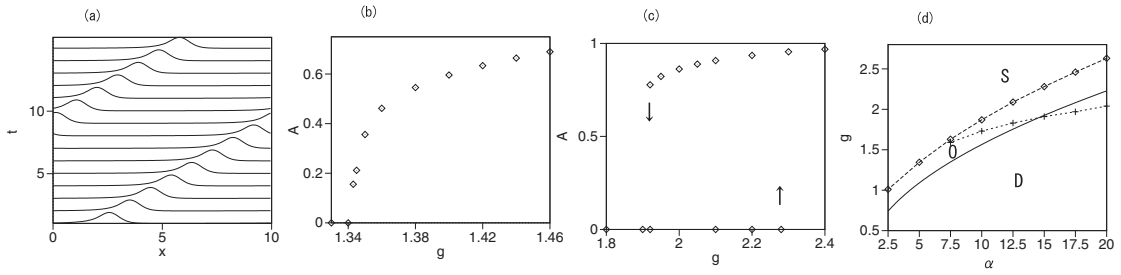

FIG. II.7: (a) Propagating solitary wave state for $L = 10$, $\alpha = 5$, and $T = 0.1$. (b) Fourier amplitude A for the local order parameter $\langle \cos \phi(x) \rangle$ as a function of g at $\alpha = 5$, $T = 0.1$, and $L = 10$. (c) Fourier amplitude A for the local order parameter $\langle \cos \phi(x) \rangle$ as a function of g at $\alpha = 15$, $T = 0.1$, and $L = 10$. (d) Phase diagram in the parameter space of (α, g).

A increases from 0 continuously at $g \simeq 1.34$. Figure II.7(c) shows the Fourier amplitude A as a function of g for $\alpha = 15$, $L_x = 10$, and $T = 0.1$. At these parameter values, A jumps from 0 to 0.95 at $g = 2.29$ when g increases, and A jumps from 0.78 to 0 at $g = 1.91$. When the initial condition is the disorderd state, the phase transition occurs at $g > 2.29$. When the initial condition is the solitary wave state, the phase transition occurs at $g < 1.91$. The transitions are discontinuous and hysteresis occurs.

Figure II.7(d) shows the phase diagram for $L = 10$ and $T = 0.1$. There are three states: a disordered state 'D', a spatially uniform ordered state 'O', and a solitary wave state 'S'. For $\alpha < 7.5$, the transitions from the disordered state to the spatially uniform ordered state, and from the spatially uniform ordered state to the solitary wave state are continuous. On the other hand, for $\alpha > 7.5$, the transition from the disordered state to the spatially uniform ordered state is continuous; however, the transition from the spatially uniform ordered state to the solitary wave state is discontinuous as denoted by the dashed line. The transition from the solitary wave state to the spatially uniform ordered state or the disordered state is denoted by the dotted line in Fig. II.7(d). When the initial state is the solitary wave state, the solitary wave state on the phase domain expands, as shown by the dotted line.

Figure II.8 shows a head-on collision of two solitary waves with slightly different amplitudes at $g = 2$, $L = 10$, $\alpha = 5$, and $T = 0.1$. The two solitary waves interpenetrate each other at the first collision. However, the amplitude difference increases at successive collisions, and only one solitary wave survives after a long time. This behavior is slightly different

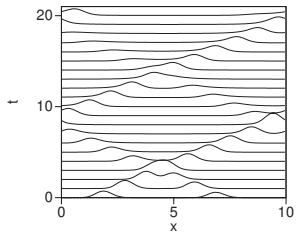

FIG. II.8: Head-on collision of two solitary waves at $g = 2$, $\alpha = 5$, $T = 0.1$, and $L_x = 10$.

from the head-on collision of two solitary waves in Section I of this Chapter's model, where merging occurred at the first collision. The reason for the difference is not clear; however, it is not so surprising because various phenomena such as pair annihilation, interpenetration, and the formation of a bound state occur at the head-on collision of two general dissipative solitons depending on the control parameters [20, 21]. This type of behavior is similar to the numerical result obtained with a model based on the kinetic theory for the Vicsek model by Ihle [17].

V. SIMPLE MODEL FOR SOLITARY WAVE STATE

The mechanism of the instability from the ordered state to the solitary wave state is still not clear. In this section, we study a simple one-dimensional model equation to understand the instability qualitatively. We assume that each self-propelled particle takes one of two velocities, v_0 or $-v_0$, and the velocity of each particle changes from v_0 to $-v_0$ with transition probability r_+ and from $-v_0$ to v_0 with transition probability r_-. Then, the probability densities $P_\pm(x)$ of velocities $\pm v_0$ obey the model equation

$$\begin{aligned} \frac{\partial P_+}{\partial t} &= -v_0 \frac{\partial P_+}{\partial x} + D\frac{\partial^2 P_+}{\partial x^2} + r_- P_- - r_+ P_+, \\ \frac{\partial P_-}{\partial t} &= v_0 \frac{\partial P_-}{\partial x} + D\frac{\partial^2 P_-}{\partial x^2} + r_+ P_+ - r_- P_-, \end{aligned} \tag{II.28}$$

where $D\partial^2 P_\pm/\partial x^2$ are artificial diffusion terms to suppress divergence. Furthermore, we assume that $r_- = e^{g(P_+ - P_-)}$ and $r_+ = e^{-g(P_+ - P_-)}$. This equation represents simple dynamics of the mean-field type Ising model if spatial uniformity is assumed. At the equilibrium state, the relation

$$\frac{P_-}{P_+} = \frac{r_+}{r_-} = e^{-2g(P_+ - P_-)} \tag{II.29}$$

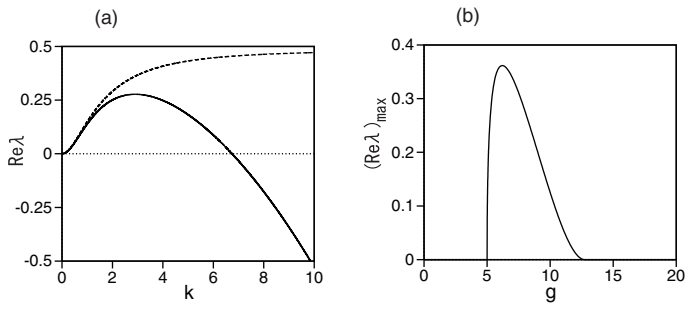

FIG. II.9: (a) Re$\lambda(k)$ as a function k for $D = 0$ and 0.01 at $g = 8$, $L = 4$, and $v_0 = 1$. (b) Peak value of Re$\lambda(k)$ as a function g for $D = 0.01$, $L = 4$, and $v_0 = 1$.

is satisfied. The spatially uniform solutions P_{0+} and P_{0-} are obtained from this self-consistent equation. If the normalization $\int_0^L (P_+(x)+P_-(x))dx = 1$ is assumed, the spatially uniform disordered state $P_{0+} = P_{0-} = 1/(2L)$ becomes unstable at $g = L$, and the spatially uniform ordered state $P_{0+} \neq P_{0-}$ appears for $g > L$. From Eq. (II.28), perturbations of the form $\delta P_+ e^{ikx+\lambda t}$ and $\delta P_- e^{ikx+\lambda t}$ obey

$$\begin{aligned} \lambda \delta P_+ &= (-ikv_0 - Dk^2 + a_{11})\delta P_+ + a_{12}\delta P_-, \\ \lambda \delta P_- &= -a_{11}\delta P_+ + (ikv_0 - Dk^2 - a_{12})\delta P_-, \end{aligned} \tag{II.30}$$

where

$$a_{11} = -e^{-g(P_{0+}-P_{0-})} + ge^{g(P_{0+}-P_{0-})}P_{0-} + ge^{-g(P_{0+}-P_{0-})}P_{0+},$$

$$a_{12} = e^{g(P_{0+}-P_{0-})} - ge^{g(P_{0+}-P_{0-})}P_{0-} - ge^{-g(P_{0+}-P_{0-})}P_{0+}.$$

The eigenvalue $\lambda(k)$ is expressed as

$$\lambda(k) = \frac{-(a_{12}-a_{11}) \pm \sqrt{(a_{12}-a_{11})^2 - 4k^2v_0^2 - 4ikv_0(a_{11}+a_{12})}}{2} - Dk^2.$$

The linear growth rate or the real part of λ can be explicity written as

$$\mathrm{Re}\lambda(k) = \frac{-(a_{12}-a_{11}) + \beta}{2} - Dk^2, \tag{II.31}$$

where

$$\beta = \left[\frac{(a_{12}-a_{11})^2 - 4k^2v_0^2 + \sqrt{\{(a_{12}-a_{11})^2 - 4k^2v_0^2\}^2 + 16k^2v_0^2(a_{11}+a_{12})^2}}{2} \right]^{1/2}. \tag{II.32}$$

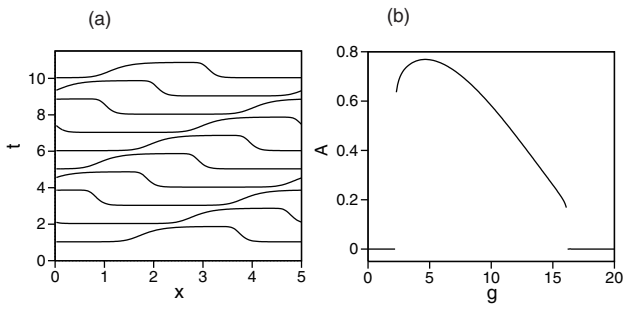

FIG. II.10: (a) Time evolution of the density $P_+ + P_-$ at $g = 8$, $L = 5$, $v_0 = 1$ and $D = 0.01$ for Eq. (II.28). (b) Fourier amplitude A of the order parameter $P_+(x) - P_-(x)$ as a function of g at $L = 5$, $v_0 = 1$, and $D = 0.01$ for Eq. (II.28).

Figure II.9(a) shows the relationship between k and Re$\lambda(k)$ for $D = 0$ and 0.01 at $g = 8$, $L = 5$, and $v_0 = 1$. The linear growth rate becomes positive, which implies that the spatially uniform state is unstable. At $k = 0$, Reλ=0. At $D = 0$, Re$\lambda \to a_{11}$ for $k \to \infty$, which can be shown using Eqs. (II.31) and (II.32). The instability originates from the terms $\mp v_0 \partial P_\pm / \partial x$ in Eq. (II.28). Figure II.9(b) shows the peak value of Re$\lambda(k)$ as a function of g for $D = 0.01$, $L = 5$, and $v_0 = 1$. The spatially uniform state is unstable for $5 < g < 12.7$.

Figure II.10(a) shows the time evolution of the density $\rho(x) = P_+(x) + P_-(x)$ at $g = 8$, $L = 5$, $v_0 = 1$, and $D = 0.01$. A propagating solitary wave state appears. The solitary wave state propagates with velocity 1.04, which is slightly larger than $v_0 = 1$. At $D = 0$, Eq. (II.28) exhibits divergence and the steadily propagating solitary wave state cannot be obtained. Figure II.10(b) shows the Fourier amplitude $A = |\int_0^L (P_+ - P_-) e^{2\pi i x/L} dx|$ of the local order parameter $P_+ - P_-$ as a function of g at $L = 5$, $v_0 = 1$, and $D = 0.01$. The solitary wave state is stable for $2.3 < g < 16.1$. The solitary wave state and the spatially uniform disordered state are bistable for $2.3 < g < 5$, and the solitary wave state and the spatially uniform ordered state are bistable for $12.7 < g < 16.1$. For $g > 16.1$, only the spatially uniform ordered state is stable. This might be related to the previous numerical results showing that the solitary wave states appear near the transition range between the disordered state and the ordered state.

We consider that the instability of the spatially uniform ordered state in Eq. (II.22) is also caused by the drift term $-\partial/\partial x(\cos\theta P)$, and that the nonlocal coupling term in Eq. (II.22) might play a role of the artificial diffusion term in Eq. (II.28) to suppress the divergence.

VI. SUMMARY

We have investigated the nonlinear Kramers equation for one-dimensional self-propelled particles. This equation is based on the mean-field approximation, which can be used in non-locally interacting systems. The deterministic nonlinear Kramers equation clarifies several problems regarding the collective motion of self-propelled particles. In the nonlinear Kramers equation, a solitary wave state appears as a stable state. The phase transition to the solitary wave state occurs even in one dimension because our model is a non-locally coupled system, and the mean-field approximation can be applied. Furthermore, we have found that the average concentration $\rho(x)$ and average velocity $u(x)$ satisfy a simple relation. An approximate solution of the solitary wave state is constructed using the self-consistent method. The transition from the disordered state to the solitary wave state becomes discontinuous, depending on the control parameters.

We consider that the solitary wave state in our one-dimensional model corresponds to the traveling band found in Vicsek's two-dimensional model because both states are solitary waves and appear near the transition point to the collective motion. We found that only one solitary wave survives after the collision in the head-on collision of two solitary waves.

We have found that the solitary wave state appears naturally in the direct numerical simulation of the nonlinear Kramers equation; however, the solitary wave state's formation mechanism is still not clarified. Interestingly, self-propelled particles gather together in the solitary wave state even though mutual attraction is absent. We have considered a qualitative mechanism of the formation of the solitary wave state using the free energy given by Eq. (II.20). Finally, we have constructed a simple one-dimensional model equation and found that the drift term causes the instability of the spatially uniform ordered state.

Chapter Ⅲ

Solitary wave states maintained by stochastic direction changes in a population of self-propelled particles

I. ONE-DIMENSIONAL ISING-TYPE VICSEK MODEL

We are interested in the flipping cluster state in the one-dimensional active Ising model (AIM). However, the phenomenon cannot be confirmed in two dimensions due to the substantial fluctuations. Other models do not study the phenomenon. We will propose and investigate a model to reproduce the phenomenon. First, we will study it with a one-dimensional model. Next, we will study it in a two-dimensional model. We call it Ising-type Vicsek model.

In the one-dimensional Ising-type Vicsek model, each particle moves on a linear lattice with velocities ± 1. The velocity of the ith particle at discrete time t is expressed as $v_{i,t}$. The position $x_{i,t+1}$ of the ith particle at t + 1 is determined by a simple rule: $x_{i,t+1} = x_{i,t} + v_{i,t+1}$. Particles in the Vicsek model move on a two-dimensional plane, while particles in the Ising-type Vicsek model move on a lattice point. The total number of particles is expressed as N. The lattice size is L, and periodic boundary conditions are assumed. Particles have no volume because of point particles. Multiple particles can occupy the same lattice site as shown in Fig. III.1. The number of right- or left-moving particles on the jth site at a discrete time t is denoted as $n_{+j,t}$ and $n_{-j,t}$. The particle number at the site j is denoted as $n_{j,t} = n^+_{j,t} + n^-_{j,t}$. The difference $m = n^+_{j,t} - n^-_{j,t}$ in the numbers of right- and left-moving particles at the site expresses a local order parameter corresponding to magnetization. In the active Ising model, each particle has a spin variable s_i, and the particle moves at rates $D(1 + s\epsilon)$ and $D(1 - s\epsilon)$ to its right and left neighboring site. The spin s is assumed to flip to $-s$ at rate $\exp(-sm_{j,t}/Tn_{j,t})$, where T is a parameter corresponding to the temperature. The particle position and the spin variable change randomly. The flipping rate is

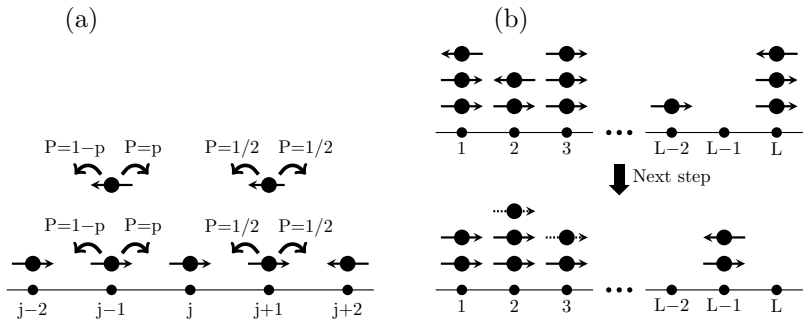

FIG. III.1: (a) Sketch of particles moving to the left or right stochastically in one-dimensional Ising-type Vicsek model. Multiple particles can occupy the same lattice site. (b) Sketch of the movement of particles in the next step. Particles move in concert in the next step. The dotted arrows show particles flipped in the next step.

determined by the ratio $m_{j,t}/n - j, t$ of the local order parameter over the local particle number. In our model, only the velocity $v_{i,t}$ is a stochastic variable, and the position at the next time step $t+1$ is determined by the velocity $v_{i,t+1}$. The particle velocity $v_{i,t} = 1$ or -1 is randomly chosen with the probability determined by the interaction with particles in the same site and the neighboring sites. That is, particle on ith site interacts with particles on $(i-1)$th, ith and $(i+1)$th sites. For a local sum of the order parameter, $m_{j,t}$ is defined as $\tilde{m}_{j,t} = m_{j,t} + q(m_{j-1,t} + m_{j+1,t})$, where q is a parameter for the strength of the nearest-neighbor coupling. For the sake of simplicity, we use $q = 1/2$ unless explicitly otherwise stated in this paper. By $\tilde{m}_{j,t}$, the probability that the ith particle on the jth site takes $v_{i,t+1} = \pm 1$ at the next time step $t+1$ is assumed to be

$$p^{\pm}_{j,t+1} = \frac{\mathrm{e}^{\pm g s_{j,t}}}{\mathrm{e}^{g s_{j,t}} + \mathrm{e}^{-g s_{j,t}}}, \tag{III.1}$$

where $s_{j,t} = 1$ for $\tilde{m}_{j,t} > 0$, $s_{j,t} = 0$ for $\tilde{m}_{j,t} = 0$, and $s_{j,t} = -1$ for $\tilde{m}_{j,t} < 0$. Particles tend to move together with the majority group with a higher probability $p_g = \mathrm{e}^g/(\mathrm{e}^g + \mathrm{e}^{-g})$ and move to the opposite direction with a smaller but finite probability $\mathrm{e}^{-g}/(\mathrm{e}^g + \mathrm{e}^{-g})$ as shown on the $(j-1)$th site in Fig. III.1(a). For $\tilde{m}_{j,t} = 0$, particles move to the left or right with probability 1/2 as shown on the $(j+1)$th site in Fig. III.1(a). Figure III.1(b) shows the one-step evolution in accordance with the updating rules. On the other hand, the probability of spin variables in AIM is determined by the local order parameter $m_{j,t}$ like $p^{\pm}_{j,t+1} = \mathrm{e}^{\pm g m_{j,t}}/(\mathrm{e}^{g m_{j,t}} + \mathrm{e}^{-g m_{j,t}})$. Since the velocity is $+1$ or -1, the average numbers

$n^+_{j+1,t+1}$ and $n^-_{j-1,t+1}$ of right- and left-moving particles at time $t+1$ are expressed as

$$\begin{aligned} n^+_{j+1,t+1} &= \frac{\mathrm{e}^{gs_{j,t}}}{\mathrm{e}^{gs_{j,t}} + \mathrm{e}^{-gs_{j,t}}} n_{j,t}, \\ n^-_{j-1,t+1} &= \frac{\mathrm{e}^{-gs_{j,t}}}{\mathrm{e}^{gs_{j,t}} + \mathrm{e}^{-gs_{j,t}}} n_{j,t}, \end{aligned} \tag{III.2}$$

where $n_{j,t} = n^+_{j,t} + n^-_{j,t}$. If $n^+_{j,t}$, $n^-_{j,t}$, $n_{j,t}$, and $s_{j,t}$ do not depend on j or the system is spatially uniform,

$$m_{t+1} = n^+_{t+1} - n^-_{t+1} = \frac{N}{L} s_t \tanh(g) \tag{III.3}$$

is satisfied. A disordered state $m_t = 0$ is possible but unstable, and the uniform state is an ordered state for any value of $g > 0$. The linear stability of the spatially uniform state in the mean-field model (III.2) can be investigated by assuming $n^+_{j,t} = (N/L)p_g + \delta n^+_k e^{ikj}(\lambda_k)^t$ and $n^-_{j,t} = (N/L)(1-p_g) + \delta n^-_k e^{ikj}(\lambda_k)^t$ where $k = 2\pi m/L$. Substitution of the ansatz into Eq. (III.2) yields

$$\delta n^+_k \lambda_k = p_g e^{-ik}(\delta n^+_k + \delta n^-_k),\ \delta n^-_k \lambda_k = (1-p_g)e^{ik}(\delta n^+_k + \delta n^-_k).$$

The linear growth rate λ_k is expressed as

$$\lambda_k = \cos k + i(1-2p_g)\sin k. \tag{III.4}$$

Since $-1 < 1-2p_g < 1$, $|\lambda_k| < 1$ and the uniform ordered state is linearly stable. That is, there is no order–disorder transition in this model. The majority rule causes this. The stability of the spatially uniform ordered state in the mean-field approximation Eq. (III.2) is characteristic of our model, which is different from the AIM and the active Potts model (APM).

Although the uniform state is stable in the mean-field approximation, a solitary wave state maintained by stochastic direction changes appears with number fluctuations. We show an example of numerical simulation in Fig. III.2. Initially, each particle is randomly set on the lattice, or $v_{i,1} = 1$ or -1 is randomly chosen. The system size is set to $L = 500$, and the total number of particles is $N = 5000$. Figure III.2(a) shows the disordered state that particles move randomly. Figures III.2(a) and III.3(b) use same parameter. Figure III.3(a) shows that small-amplitude peaks appear frequently. Particles do not make a cluster. Figure III.2(b) shows the ordered state that particles move in concert. Figures III.2(b) and III.3(b) use same parameter. Figure III.3(b) shows that the particles moving to the right are almost uniformly

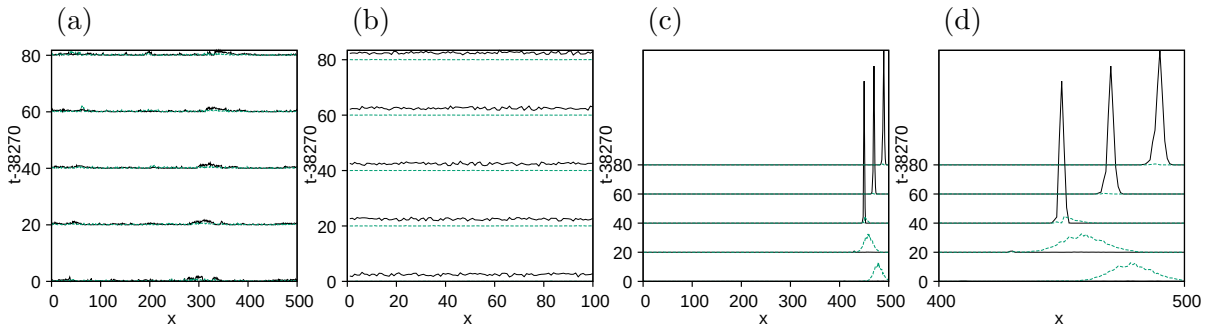

FIG. III.2: Time evolutions of the profiles $n^+_{j,t}$ (solid black line) and $n^-_{j,t}$ (dashed green line) from $t = 38270$ to 38350 at $N = 5000$. (a) The disordered state. Parameters: $L = 500$ and $g = 0.5$. (b) The ordered state. Parameters: $L = 100$ and $g = 2.5$. (c) Flipping solitary wave state. Parameters: $L = 500$ and $g = 2.5$. The solitary wave moves toward the left at $t = 38270$. The small wave (black line) appears and collides the large wave (green line) around $t = 38290$. The small wave swallows up it around $t = 38310$. (d) The enlarged view of Fig. III.2(c).

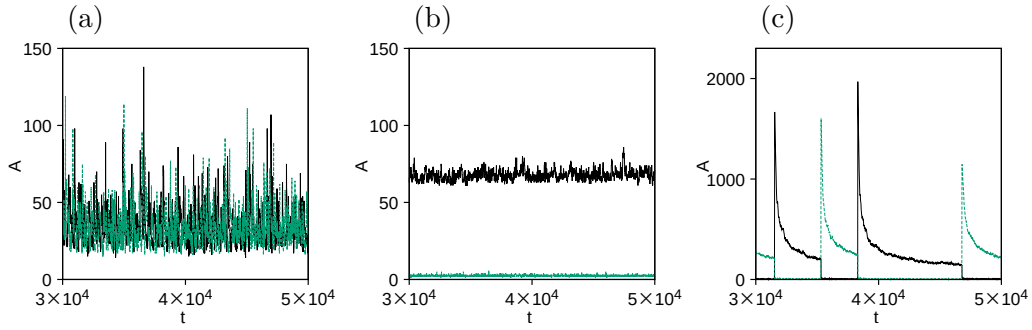

FIG. III.3: Time evolutions of the peak amplitudes A of $n^+_{j,t}$ (solid black line) and $n^-_{j,t}$ (dashed green line) at $N = 5000$. (a) Disordered state. Parameters: $L = 500$ and $g = 0.5$. (b) Ordered state. Parameters: $L = 100$ and $g = 2.5$. (c) Flipping solitary wave state. Parameters: $L = 500$ and $g = 2.5$.

distributed in space. Figure III.2(c) shows a transition process from a left-traveling solitary wave to a right-traveling solitary wave at $g = 2.5$. It is seen that the amplitude of the left-traveling solitary wave (green line) is fairly small, around $t = 84000$, before the transition, and the right-traveling solitary wave (blue line) with very high amplitude suddenly appears at $t = 84050$. Figure III.2(d) shows the detailed time evolution of the profiles of $n^+_{j,t}$ (blue

line) and $n^-_{j,t}$ (green line) near the transition time. A broad solitary wave moves to the left at $t < 84010$. Almost all particles are included in this left-moving solitary wave. Owing to fluctuation, a right-traveling solitary wave of small amplitude appears near $i = 276$ in front of the left-traveling solitary wave at around $t = 84002$. The left-traveling solitary wave collides with the right-traveling solitary wave of small amplitude. The waves invariably collide head-on in a one-dimensional system since particles only move to the left or right. Since the peak position of the right-traveling solitary wave is higher than that of the left-traveling solitary wave at the colliding position, the peak amplitude of the right-traveling solitary wave increases rapidly by swallowing the left-traveling particles. After the right-traveling solitary wave passes over the broad left-traveling wave, the left-traveling solitary wave almost disappears. As a result, the right-traveling narrow solitary wave with a very large amplitude appears. We call this phenomenon the sweeping-up process in this paper. By this process, the minor changes to the majority quickly. The process finishes with a single collision in a one-dimensional system.

The peak amplitude of the surviving right-traveling solitary wave decreases slowly, and the solitary wave becomes broad after a long time [45]. Figure III.3(c) shows the time evolutions of the peak amplitudes A of $n^+_{j,t}$ (purple line) and $n^-_{j,t}$ (yellow line) at $g = 2.5$. Here, the peak amplitudes denote the maximum values of $n^+_{j,t}$ (solid black line) and $n^-_{j,t}$ (dashed green line) with respect to j. The peak amplitude takes a maximum value of 1100–2000 just after the transition of the moving direction and decreases gradually. This implies that a very sharply localized structure is generated just after the transition of the moving direction, and then the localized structure becomes wider with time. When the peak amplitude A decreases to 140–240, another transition of the moving direction occurs. The transitions repeat repeatedly, and this repetition of direction changes maintains the solitary wave state.

II. QUALITATIVE EXPLANATION OF SWEEPING-UP PROCESS

This section tries to understand why the sweeping-up process continues qualitatively using a simpler model. Furthermore, we want to understand why the rapid transition of the moving direction occurs when the peak amplitude A decreases to 140–240.

The abrupt turning occurs with the sequential sweeping-up process after the nucleation

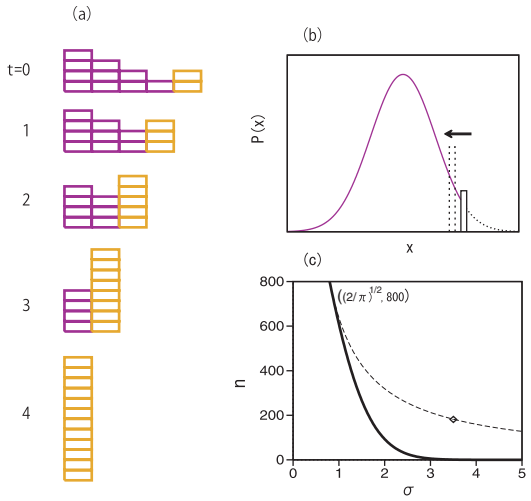

FIG. III.4: (a) Schematic sweeping-up process. (b) Number density of stationary particles expressed by the Gaussian function $n_x^0 = \bar{N}/(\sqrt{2\pi}\sigma)e^{-x^2/(2\sigma^2)}$ for $x < x_0$ and that of left-moving particles is expressed as $n_{x_0+1}^- = \bar{N}/(\sqrt{2\pi}\sigma)\int_{x_0}^{\infty} e^{-x^2/(2\sigma^2)}dx$. (c) Solid thick line: relationship between σ and $n_c^0 = \bar{N}/(\sqrt{2\pi}\sigma)e^{-x_c^2/(2\sigma^2)}$ at the critical position for $\bar{N} = 1600$. Dashed line: relationship between σ and the peak value $\bar{N}/(\sqrt{2\pi}\sigma)$ for $\bar{N} = 1600$. The marked point is (σ, n) where $\sigma = 3.5$ and $\bar{N}/(\sqrt{2\pi}\sigma)$.

of a seed of an inversely propagating wave. The sweeping-up process is simply explained as shown in Fig. III.4(a). For simplicity, we consider a toy model that has left-moving particles with velocity -1 (yellow) and stationary particles (blue) instead of right-moving particles considered in the previous section. The majority rule of $p_g = 1$ and $q = 0$ is assumed at each lattice point. That is, a stationary particle changes into a left-moving particle if the number of left-moving particles is larger than that of stationary particles, and a left-moving particle changes into a stationary particle if the number of stationary particles is larger than that of left-moving particles. The initial configuration is shown in the top panel of Fig. III.4(a). The total number of stationary particles is 10, and that of left-moving particles is 2. The majority rule is applied at each lattice point when the different types of particles are mixed. In Fig. III.4(a), left-moving particles win the game at the right end, stationary particles turn to left-moving particles, and the yellow tower of left-moving particles piles up sequentially. A very sharp surge of left-moving particles develops and swallows the stationary particles. This is a sweeping-up effect in our model.

Next, we consider a reason why the sweeping-up process occurs sequentially using a Gaussian function. That is, the number distribution of stationary particles is expressed with a Gaussian function, and the majority game of $p_g = 1$ and $q = 0$ between the stationary and left-moving particles is considered as in the previous paragraph. The total number of particles is assumed to be $\bar{N}$. The initial number density of stationary particles is assumed to be expressed with the Gaussian function as $n_x^0 = \bar{N}/(\sqrt{2\pi}\sigma)e^{-x^2/(2\sigma^2)}$ for $x \leq x_0$ for a certain lattice point x_0. The particle number of stationary particles is approximated at $n_x^0 \Delta x = n_x^0$ where $\Delta x = 1$ is the lattice interval. The number of the left-moving particles is evaluated as $\bar{N} - \int_{-\infty}^{x_0} \bar{N}/(\sqrt{2\pi}\sigma)e^{-y^2/(2\sigma^2)}dy = \int_{x_0}^{\infty} \bar{N}/(\sqrt{2\pi}\sigma)e^{-y^2/(2\sigma^2)}dy$, and all the left-moving particles are assumed to be set at a lattice point $x_0 + 1$ neighboring to x_0 and therefore $n_{x_0+1}^- = \bar{N}/(\sqrt{2\pi}\sigma)\int_{x_0}^{\infty} e^{-y^2/(2\sigma^2)}dy$ as shown in Fig. III.4(b). If the left-moving particles move to x_0 at the next time-step, win the majority game, and swallow the stationary partilces located at $x = x_0$, the number of left-moving particles at $x = x_0$ is expressed as $n_{x_0}^- = \bar{N}/(\sqrt{2\pi}\sigma)\int_{x_0-1}^{\infty} e^{-y^2/(2\sigma^2)}dy$. If the sweeping-up process by the left-moving particles reaches the lattice point $x_1 + 1$ satisfying $x_1 + 1 \leq x_0$, the number of stationary particles is expressed $n_x^0 = \bar{N}/(\sqrt{2\pi}\sigma)e^{-x^2/(2\sigma^2)}$ for $x \leq x_1$, and the number of left-moving particles at $x = x_1 + 1$ is expressed as $n_{x_1+1}^- = \bar{N}/(\sqrt{2\pi}\sigma)\int_{x_1}^{\infty} e^{-y^2/(2\sigma^2)}dy$.

To consider the sequential occurrence of the sweeping-up process, we define a function $F(x)$:

$$F(x) = e^{-x^2/(2\sigma^2)} - \int_x^{\infty} e^{-y^2/(2\sigma^2)}dy.$$

There is a critical value x_c satisfying

$$F(x_c) = e^{-x_c^2/(2\sigma^2)} - \int_{x_c}^{\infty} e^{-y^2/(2\sigma^2)}dy = 0. \tag{III.5}$$

The function $F(x)$ has a property that $F'(x) = -x/\sigma^2 + e^{-x^2/(2\sigma^2)} > 0$ for $x < x_c$, and $F(x_1) < F(x_0) < F(x_c) = 0$ for $x_1 < x_0 < x_c$. This result implies that the sweeping-up process occurs sequentially if $x_0 < x_c$ is satisfied, because $n_{x_1}^0 = \bar{N}/(\sqrt{2\pi}\sigma)e^{-x_1^2/(2\sigma^2)} < \bar{N}/(\sqrt{2\pi}\sigma)\int_{x_1}^{\infty} e^{-x^2/(2\sigma^2)}dx = n_{x_1+1}^-$ is always satisfied for any lattice point x_1 satisfying $x_1 < x_0 < x_c$ and the left-moving particles always win the majority game. On the other hand, if $x_0 > x_c$, the sweeping-up process does not ignite.

The critical position x_c can be numerically calculated from Eq. (III.5) as a function of σ. $\bar{N}$ is assumed to be $\bar{N} = 1600$ from a rough estimate of the local maximum values of the peak amplitude A in Fig. III.3(c), since the peak amplitude increases to the maximum value $\bar{N}$

in the sweeping-up process using the Gaussian function. The solid thick line in Fig. III.4(c) shows a relationship between σ and $n_c^0 = \bar{N}/(\sqrt{2\pi}\sigma)e^{-x_c^2/(2\sigma^2)}$ at the critical position x_c for $\bar{N} = 1600$. The solid thick line starts at $\sigma = \sqrt{2/\pi}$ and $n_c^0 = \bar{N}/2 = 800$ where x_c becomes 0. It is easily checked that $x_c = 0$ and $\sigma = \sqrt{2/\pi}$ are the solution to Eq. (III.5), since the right-hand side is $\bar{N}/2$ for $x_c = 0$, and there is no solution for $\sigma < \sqrt{2/\pi}$ to Eq. (III.5).

As σ decreases, the critical number n_c^0 increases as shown by the solid thick line in Fig. III.4(c). If the number of left-moving particles is larger than n_c^0 at the critical position x_c, the sweeping-up ignites. Although we assumed that all the left-moving particles are initially set at the site neighboring the cluster of stationary particles in the previous paragraph, left-moving particles are generated from the majority particles with the probability $1 - p_g$ in numerical simulations of $p_g < 1$. When the width σ of the number distribution of the majority particles is small, the sweeping-up process hardly ignites because the number of left-moving particles hardly goes over the large critical number n_c^0 for small σ. On the other hand, left-moving particles always appear with a small probability $1 - p_g$ from the majority group in the Ising-type Vicsek model, n_{j+1}^- can take one or two for any j by the fluctuation effect. Therefore, it becomes possible that $n_{x_c+1}^-$ takes a value larger than $n_{x_c}^0$ and the sweeping-up ignites when $n_{x_c}^0$ becomes nearly 1. This point is considered the actual critical position x_c for the occurrence of the stochastic direction change. In our simple model, the critical number density $n_c^0(x_c)$ takes 1 near $\sigma = 3.5$ for $\bar{N} = 1600$. The dashed line in Fig. III.4(c) shows the peak value $\bar{N}/(\sqrt{2\pi}\sigma)$ of the Gaussian function as a function of σ. For $\sigma = 3.5$, the peak value is around 180, which is the same order as the minimum values 140–240 of the peak amplitude A in Fig. III.3(c) just before the change of hte moving direction. When the probability distribution spreads and σ becomes the order of 3.5. That is, the peak value at $x = 0$ decreases from the maximum value 1100–2000 and reaches around 140–240, the nucleation of particles moving in the opposite direction occurs, and the sweeping-up process ignites.

III. NUMBER FLUCTUATIONS AND STOCHASTIC COUPLED MAP LATTICE MODEL

This section will discuss in more detail the importance of number fluctuations for the nucleation of particles moving in the opposite direction. In the mean-field approximation

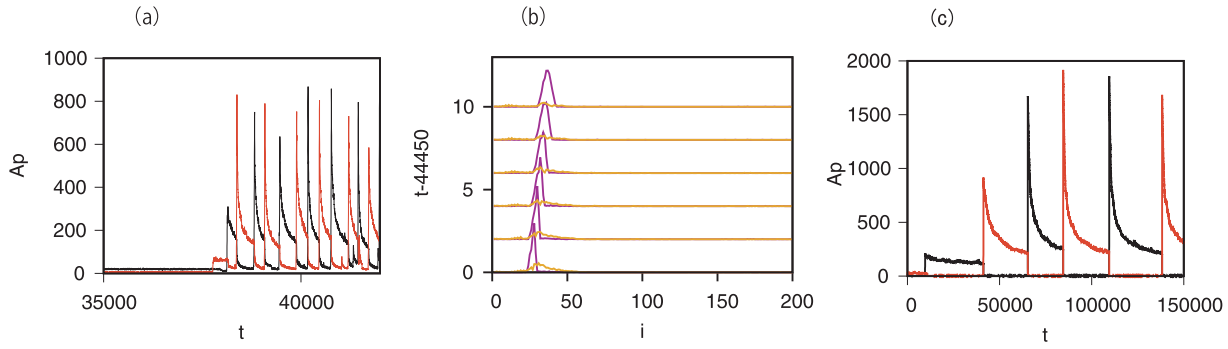

FIG. III.5: (a) Time evolutions of the peak amplitudes of $n^+_{j,t}$ (black) and $n^-_{j,t}$ (red) at $g = 1$, $L = 500$, and $N = 5000$ starting from the ordered state. (b) Time evolutions of the profiles of $n^+_{j,t}$ (purple) and $n^-_{j,t}$ (yellow) at $g = 1$ near $t = 44450$. (c) Time evolutions of the peak amplitudes of $n^+_{j,t}$ (black) and $n^-_{j,t}$ (red) at $g = 3.5$, $L = 5000$, and $N = 5000$ starting from the ordered state.

described by Eq. (III.2) for the Ising-type Vicsek model, the spatially uniform ordered state is linearly stable and the spatially uniform ordered state is finally obtained as shown later in Fig. III.6(a). However, the solitary wave state appears and is maintained stably by changing the moving direction, when the initial condition is random. Even if the initial condition is the ordered state, the solitary wave state maintained by direction changes appears owing to the number fluctuations.

Figure III.5(a) shows the time evolutions of the peak amplitudes A of $n^+_{j,t}$ (black) and $n^-_{j,t}$ (red) at $g = 1$ and $L = 500$ and $N = 5000$ starting from an initial condition of all right-moving particles. Here, g is the parameter governing the conformity to the majority. Initially, a uniform ordered state with $A \simeq N/L = 10$ appears; however, the ordered state changes to the solitary wave state maintained by direction changes near $t = 37770$. Figure III.5(b) shows the time evolution of the profiles of $n^+_{j,t}$ (purple) and $n^-_{j,t}$ (yellow) near $t = 44450$ in the numerical simulation shown in Fig. III.5(a). A solitary wave propagates in the right direction in this time range. The uniform ordered state was maintained for a longer time at a larger value of g because the probability $1 - p_g$, generating minority particles becomes smaller. Even when the average number is 10 in the spatially uniform state, it is very difficult for the particle number of the minority generated by the small probability $1 - p_g$ to exceed the average number 10 for large g. For example, the uniform state was maintained until $t = 10^6$ at $g = 1.5$. Number fluctuations become more important when

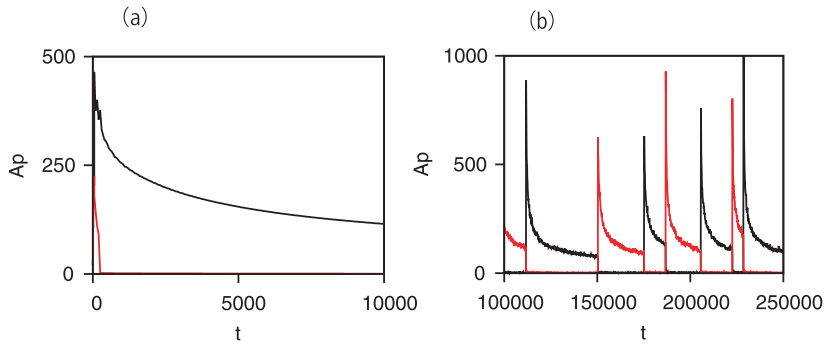

FIG. III.6: (a) Time evolution of the peak amplitudes of $n^+_{j,t}$ (black line) and $n^-_{j,t}$ (red line) at $g = 2.5$, $L = 500$, and $N = 5000$ calculated by Eq. (III.6) without the noise terms. (b) Time evolution of the peak amplitudes of $n^+_{j,t}$ (black line) and $n^-_{j,t}$ (red line) at $g = 2.5$, $L = 500$, and $N = 5000$ calculated by Eq. (III.6).

the average number density becomes smaller by increasing the system size. Figure III.5(c) shows the time evolutions of the peak amplitudes of $n^+_{j,t}$ (black) and $n^-_{j,t}$ (red) at a very large value $g = 3.5$ for $L = 5000$ and $N = 5000$ starting from the initial condition of all right-moving particles. The flipping cluster state appears easily even at $g = 3.5$ because the average number density is 1. Therefore $n^-_{j,t}$ can easily take 1, and $\tilde{m}_{j,t}$ takes a negative value with the number fluctuations.

Equation (III.2) was derived by neglecting the effect of number fluctuations. The fluctuation effect can be incorporated by adding noise terms in Eq. (III.2) as

$$\begin{aligned} n^+_{j+1,t+1} &= \frac{e^{gs_{j,t}}}{e^{gs_{j,t}} + e^{-gs_{j,t}}} n_{j,t} + \xi_{j,t}, \\ n^-_{j-1,t+1} &= \frac{e^{-gs_{j,t}}}{e^{gs_{j,t}} + e^{-gs_{j,t}}} n_{j,t} - \xi_{j,t}, \end{aligned} \tag{III.6}$$

where $\xi_{j,t}$ is Gaussian white noise with variance $\sigma^2 = n_{j,t}p_g(1-p_g)$. Equation (III.6) has the form of a stochastic coupled map lattice. The first terms on the right-hand sides in Eq. (III.6) denote the average number of right- or left-moving particles at site j and time t, and the second terms expresses the effect of number fluctuations. The variance formula $\sigma^2 = np(1-p)$ of the binomial distribution taking two choices with probabilities p_g and $1-p_g$ for the trial number n is used. Figure III.6(a) shows the time evolution of the peak amplitudes of $n^+_{j,t}$ (black line) and $n^-_{j,t}$ (red line) at $g = 2.5$ and $L = 500$ calculated by Eq. (III.6) without the noise terms. The peak amplitude of $n^+_{j,t}$ (black) goes to the

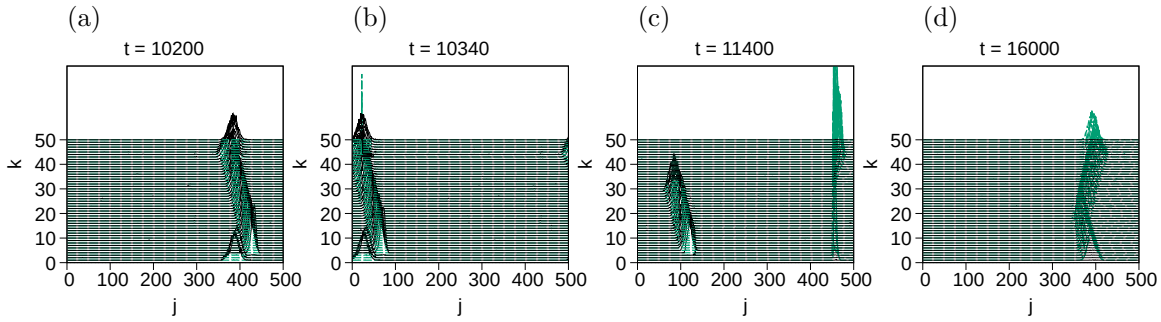

FIG. III.7: Four snapshot patterns of flip motion of solitary wave. Parameters: $L_x \times L_y = 500 \times 50$, $N = 2.5 \times 10^5$, $g = 2.8$. (a) solitary wave moving in the right (solid black line) at $t = 10200$. (b) The onset of flip motion at $t = 10340$. The high peak wave moving in the left (dashed green line) swallows particles on neighbor rows over time. (c) the coexistence of two waves at $t = 11400$. (d) Solitary wave moving in the left (dashed green line) after flip motion at $t = 16000$.

uniform value and $n^-_{j,t}$ (red) decays to zero rapidly at $t \simeq 200$. Figure III.6(b) shows the time evolution of the peak amplitudes of $n^+_{j,t}$ (black line) and $n^-_{j,t}$ (red line) at $g = 2.5$ and $L = 500$ calculated by Eq. (III.6). The solitary wave state maintained by direction changes appears in Eq. (III.6), and the change in the characteristics change of the peak amplitude is observed. This numerical simulation suggests that the nucleation of seeds of inversely moving particles through fluctuations and the sweeping-up effect are important for our model's solitary wave state.

IV. ISING-TYPE VICSEK MODEL ON SQUARE LATTICE

The Ising-type Vicsek model can be generalized to a two-dimensional system. This section considers the two-dimensional Ising-type Vicsek model on a square lattice. In the two-dimensional model, particles are randomly set on a rectangular lattice of $L_x \times L_y$, and the velocity takes one of two values $+1$ and -1 randomly as an initial condition. Periodic boundary conditions are assumed in the x direction (horizontal direction). For the interaction, the local sum of order parameter on (j,k)th site at time t is defined as $\tilde{m}_{j,k,t} = m_{j,k,t} + q(m_{j-1,k-1,t} + m_{j-1,k,t} + m_{j+1,k,t} + m_{j,k-1,t} + m_{j,k+1,t})$, where $m_{j,k,t} = n^+_{j,k,t} + n^-_{j,k,t}$, and $q = 1/2$. No-flux boundary conditions such as $n^+_{j,L_y+1,t} = n^+_{j,L_y,t}$ and $n^-_{j,0,t} = n^-_{j,1,t}$ are

assumed in the y direction for the calculation of $\tilde{m}_{j,k,t}$. If $\tilde{m}_{j,k,t} > 0$, then the velocity of a particle at (j,k)th site takes +1 at the next time step t+1 with probability $p^+ = e^g/(e^g+e^{-g})$ and -1 with probability $p^- = e^{-g}/(e^g + e^{-g})$ similarly to the one-dimensional model.

We have performed numerical simulation in a rectangle of system size $L_x \times L_y = 500 \times 50$. In each row, there are N = 5000 particles; therefore, the total number of particles is $5000 \times 50 = 250000$. Particles do not move to different rows, because the velocity takes only +1 or -1. Figure III.8 shows four snapshots in the turning process at (a) t = 10200, (b) 10340, (c) 11400, and (d) 16000 for g = 2.8. Figure III.8(a) shows a band-like solitary wave (black) moves in the right at $t = 10200$. Figure III.8(b) shows a very sharp left-traveling solitary wave (green) appears; the regime change occurs locally near $k = 40$ at $t = 10340$. The turning process extends in the y direction or the sharp left-traveling solitary wave extends to the neighboring k sites as shown in Fig. III.8(c). It takes some time for the velocity-turning process to complete in the y direction. Finally, another band-like soliton appears. Figure III.8(d) shows a left-traveling solitary wave (green) at t = 16000.

V. ISING-TYPE VICSEK MODEL WITH DIFFUSION ON SQUARE LATTICE

The flipping cluster states did not appear in the two-dimensional active Ising model. In the previous section, we showed that the direction-changing process repeats in the two-dimensional Ising-type Vicsek model where each particle moves only in the right or left direction and interacts with particles at the five neighboring sites [45]. In this section, we consider Ising-type Vicsek model with the vertical diffusion for moving direction on two dimensions. In the two-dimensional model, particles are randomly set on a rectangular lattice of $L_x \times L_y$; the velocity takes one of two values +1 and -1 randomly as an initial condition. Periodic boundary conditions are assumed in the x and y directions. The local sum of order parameter on (j,k)th site at time t is defined as $\tilde{m}_{j,k,t} = m_{j,k,t} + q(m_{j-1,k-1,t} + m_{j,k-1,t} + m_{j+1,k-1,t} + m_{j-1,k,t} + m_{j+1,k,t} + m_{j-1,k+1,t} + m_{j,k+1,t} + m_{j+1,k+1,t})$, where $q = 1$. The local sum of diffusion parameter is defined as $\check{m}_{j,k,t} = \{(m_{j-1,k,t} + m_{j,k,t} + m_{j+1,k,t}) - (m_{j-1,k-1,t} + m_{j,k-1,t} + m_{j+1,k-1,t} + m_{j-1,k+1,t} + m_{j,k+1,t} + m_{j+1,k+1,t})/2\}/\{(m_{j-1,k,t} + m_{j,k,t} + m_{j+1,k,t}) + (m_{j-1,k-1,t} + m_{j,k-1,t} + m_{j+1,k-1,t} + m_{j-1,k+1,t} + m_{j,k+1,t} + m_{j+1,k+1,t})/2\}$. For $\check{m}_{j,k,t} > 0$, the particle on (j,k) moves with the diffusion probability $p_D = D\check{m}_{j,k,t}$ to the upper $(j,k+1)$ or lower $(j,k-1)$ lattice points, where D is diffusion parameter. If $D = 0$, it

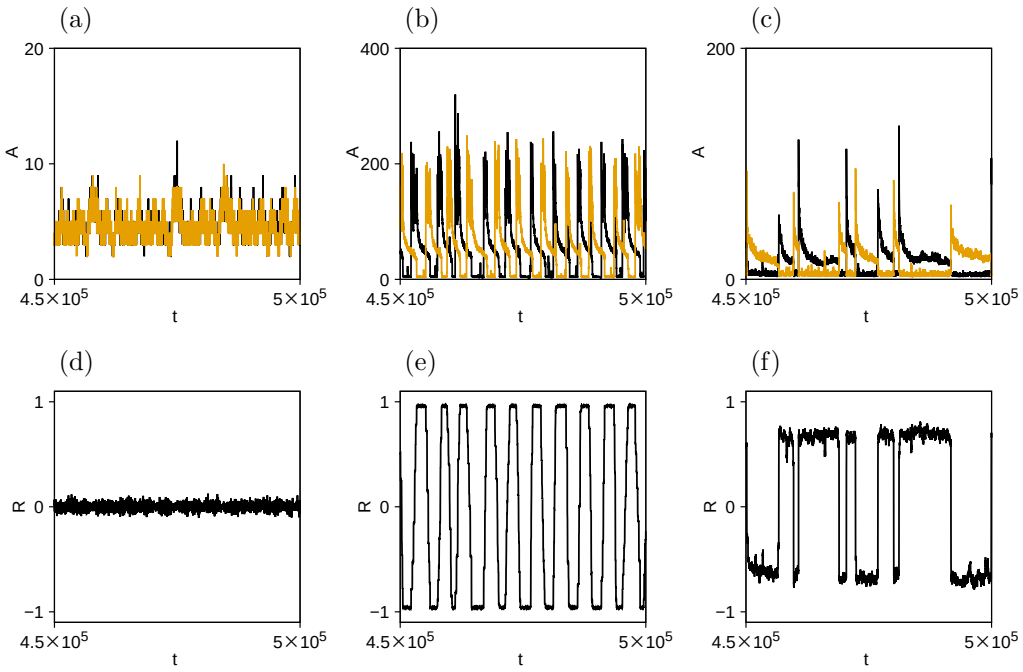

FIG. III.8: Time evolutions of the peak amplitudes A of $n^+_{i,j,t}$ (black) and $n^-_{i,j,t}$ (yellow) at $L_x \times L_y = 500 \times 50$, $N = 5 \times 10^4$. (a) Disordered state. Parameters: $g = 0.5$, $D = 0.2$. (b) Flipping solitary wave state. Parameters: $g = 2.0$, $D = 0$. (c) Flipping solitary wave state. Parameters: $g = 2.0$, $D = 0.2$. Time evolutions of the ratio $R = \sum_{i,j}(n^+_{i,j,t} - n^-_{i,j,t})/N$. (d) Disordered state. Parameters: $g = 0.5$, $D = 0.2$. (e) Flipping solitary wave state. Parameters: $g = 2.0$, $D = 0$. (f) Flipping solitary wave state. Parameters: $g = 2.0$, $D = 0.2$.

corresponds to the model without the diffusion.

We have performed a numerical simulation of system with $Lx \times Ly = 500 \times 50$ and the total number of particles is $N = 50000$. Figures III.8(a)-(c) show time evolutions of the peak amplitudes A of $n^+_{j,t}$ (black) and $n^-_{j,t}$ (yellow). Figures III.8(d)-(f) show time evolutions of the ratio $R = \sum_{i,j}(n^+_{i,j,t} - n^-_{i,j,t})/N$. Figures III.8(a) and (d) show particles move randomly. For R = 0, the total number of particles moving to the right equals the total number of particles moving to the left. Figure III.8(b) shows the higher number of directional changes of the particles than Fig. III.8(c). When the diffusion ($D = 0.2$) is introduced, the time intervals for the particles to change direction slow down. Figure III.8(e) shows R takes higher values than Fig. III.8(f). That is, the aliment rate of the direction of motion of particles is higher. However, Fig. III.8(f) shows that the changes of R from positive to negative and vice versa

are fast compared to Fig. III.8(e) and seem discontinuous. The time interval for alignment is shorter in Fig. III.8(f) than in Fig. III.8(e).

VI. POTTS-TYPE VICSEK MODEL ON TRIANGULAR LATTICE

This section considers a two-dimensional model on a triangular lattice and shows that the stochastic direction-changing process maintains the two-dimensional solitary wave state. Like the active Potts model, there are multiple moving directions in two dimensions, and thus we call it a Potts-type Vicsek model.

On the triangular lattice, each particle can move to the neighboring six sites, that is, there are six moving directions $\theta = 2\pi \cdot k/6$ $(k = 0, 1, \cdots, 5)$ as shown in Fig. III.9(a). $n^k_{i,j,t}$ is the number of particles moving in the direction $2\pi k/6$ at the (i, j) site and time t. After all particles move toward their moving direction, the majority direction $\theta_{i,j,t+1}$ is determined at each lattice point (i, j) as the maximum of $n^k_{i,j,t+1}$ with respect to k. Here, the x and y coordinates of a triangular lattice point denoted by (i, j) are expressed as $x = i$, $y = (\sqrt{3}/2)j$ for $j = 1, 3, 5, \cdots$ and $x = i + 1/2, y = (\sqrt{3}/2)j$ for $j = 2, 4, 6, \cdots$. The particles located at the lattice point are assumed to move in the majority direction $\theta_{i,j,t+1}$ with probability $p_g = e^g/(e^g + e^{-g})$, and move along $\theta_{i,j,t+1} \pm \pi/3$ with probability $(1/2)(1 - p_g) = (1/2)e^{-g}/(e^g + e^{-g})$. Multiple particles can occupy the same site similarly to the one-dimensional Ising-type Vicsek model. The periodic boundary conditions are imposed. The particle number of moving direction $k\pi/3$ at the (i, j) site at time t is denoted as $n^k_{i,j,t}$. Figure III.9(b) shows the time evolutions of the particle number ratio $R^k = \sum_{i,j} n^k_{i,j,t}/N$ for the six moving directions $(k = 0, 1, \cdots, 5)$ at $g = 3$. The system size is 301×350 and the total number of particles is $301 \times 350 = 105350$. The numbers in Figs. III.9(b) and III.9(c) denote k for the maximum of R^k with respect to k. As an initial condition, particles are randomly distributed on the triangular lattice, and the initial velocity is also random. A two-dimensionally localized structure appears after a transient time. In the solitary wave state, R^k is almost 1 for a certain k and $R^{k'}$ is almost 0 for $k' \neq k$, which implies that almost all particles move toward the direction $\theta = 2\pi k/6$. Figure III.9(b) shows that the moving direction changes rapidly compared with the time scale of the period of direction change, which is similar to the case in the one-dimensional Ising-type Vicsek model. Figure III.9(c) shows the maximum value of $n^k_{i,j,t}$ with respect to the lattice points

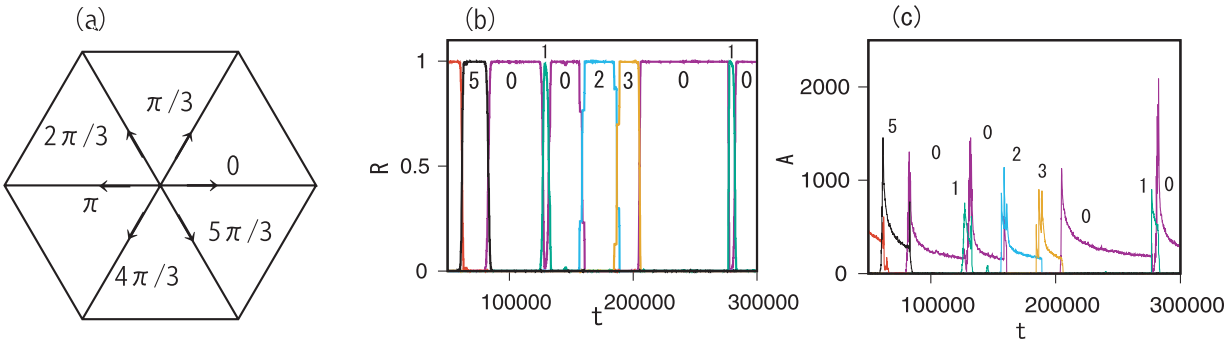

FIG. III.9: (a) Sketch of a particle moving in one of six directions. (b) Time evolutions of the particle number ratio $R^k = \sum_{i,j} n^k_{i,j,t}/N$ for the six moving directions at $g = 3$. The system size is 301×350 and the total number of particles is $301 \times 350 = 105350$. The numbers denote k for the maximum of R^k with respect to k. (c) Maximum value A of $n^k_{i,j,t}$ for the six moving directions.

for the six moving directions. A very sharply localized solitary wave appears just after the regime change in direction, and the peak amplitude decays slowly. After a while, a small new cluster of different moving directions is nucleated, invades the cluster of the major population rapidly, and grows to a new majority group. Figure III.10 shows three snapshot patterns corresponding to the transition from $\theta = 2\pi/3$ ($k = 2$) to $\theta = \pi$ ($k = 3$). In Fig. III.10(a), the green cluster moves in the $\theta = 2\pi/3$ direction. After $t = 184300$, a small spot of particles moving in the π direction appears and swallows most particles moving in the $2\pi/3$ direction. Figure III.10(b) shows a snapshot plot of the invading process of a small spot of $\theta = \pi$ (blue) around $i \simeq 200$ and $j \simeq 260$ into the large cluster of $\theta = 2\pi/3$ (green). The invading process finishes after multiple collisions. A small cluster cannot invade most particles at once because it is small in radius. The time interval of the invasion process is much shorter than the duration of one solitary wave. In Fig. III.10(c), the blue cluster wins the majority game and is moving in the π direction. The shape is irregular at this time. However, the blue cluster spreads, and the shape becomes smoother with time. The cluster assumes a two-dimensionally localized structure, which is different from the quasi-one-dimensional band structure found in the two-dimensional AIM and APM. A corresponding stochastic coupled map lattice model can be constructed. At the first step, the particle number $n'^k_{i,j,t+1}$

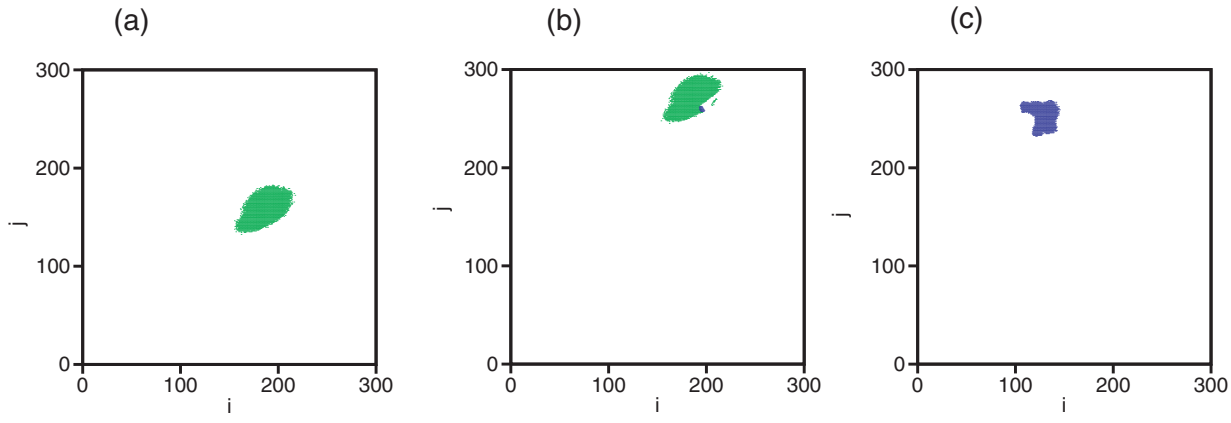

FIG. III.10: Three snapshots of patterns of $2\pi/3$ particles (green) and π particles (blue) at (a) $t = 184300$, (b) $t = 184430$, and (c) $t = 189000$. Lattice points of $n^k_{i,j,t} \geq 5$ are plotted with the color for k.

just after the majority game at the (i, j) site for the moving direction $k\pi/3$ is determined as

$$\begin{aligned} n'^{k}_{i,j,t+1} &= \frac{e^g}{e^g + e^{-g}} n_{i,j,t} + \xi_{i,j,t}, \\ n'^{k+1}_{i,j,t+1} &= \frac{e^{-g}}{2(e^g + e^{-g})} n_{i,j,t} - \frac{\xi_{i,j,t}}{2} + \eta_{i,j,t}, \\ n'^{k-1}_{i,j,t+1} &= \frac{e^{-g}}{2(e^g + e^{-g})} n_{i,j,t} - \frac{\xi_{i,j,t}}{2} - \eta_{i,j,t}, \end{aligned} \tag{III.7}$$

where $k\pi/3$ is assumed to be the moving direction of the majority group for site (i, j) and time t, and $n_{i,j,t} = \sum_{k=0}^{5} n^k_{i,j,t}$ is the particle number at the (i, j) site. At the next step, the configuration $\{n^k_{i,j,t+1}\}$ at the next time $t + 1$ is determined by the movement of $\{n'^k_{i,j,t+1}\}$ by one lattice toward the direction $k\pi/3$. The noise strength is assumed as $\langle \xi^2_{i,j,t} \rangle = n_{i,j,t} p_0 (1 - p_0)$ and $\langle \eta^2_{i,j,t} \rangle = n_{i,j,t}(1 - p_0)/4$ owing to the variance formula of the trinomial distribution.

Figure III.11(a) shows the time evolution of the maximum value A of $n^k_{i,j,t}$ with respect to the lattice points for the six moving directions when the noise strength is zero for Eq. (III.7). Different colors denote different k's. The initial configuration and the parameter g are the same as the ones in Figs. III.9 and III.10. When the noise terms are neglected, a uniform state of $k = 4$ appears after a transient time. Figure III.11(b) shows the time evolution of the maximum value A of $n^k_{i,j,t}$ with respect to the lattice points for the six moving directions when the stochasticity is involved in Eq. (III.7). The moving direction changes with time,

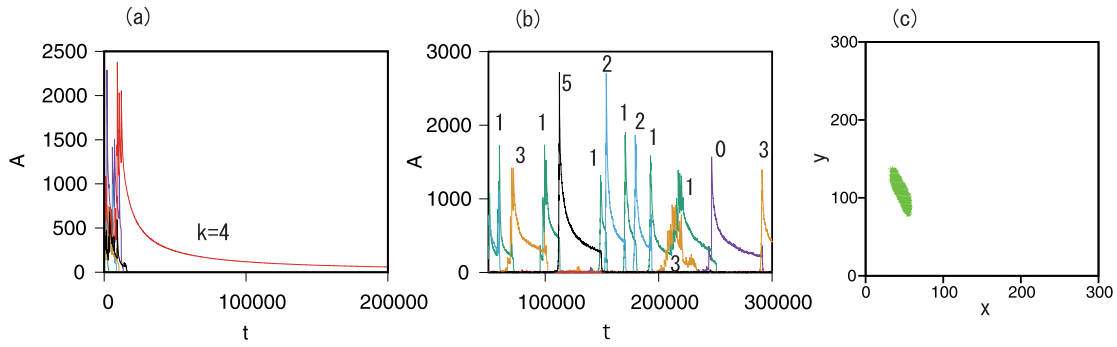

FIG. III.11: (a) Time evolution of the maximum value A of $n^k_{i,j,t}$ for the six moving directions when the noise strength is zero in Eq. (III.7). The red line denotes the maximum value for $k = 4$. (b) Time evolution of the maximum value A of $n^k_{i,j,t}$ for the six moving directions when noise terms are included. Different colors denote the maximum values for different k's. (c) Localized state for moving direction π ($k = 3$) at $t = 300000$. Lattice points of $n^k_{i,j,t} \geq 5$ are plotted with the color for $k = 3$.

and a very sharply localized cluster appears just after the direction change. Figure III.11(c) shows a localized cluster of $k = 3$ at $t = 300000$. Thus, it was shown that the nucleation of particles moving to a different direction by fluctuations and the sweeping-up effect are important for forming the solitary wave state even in two dimensions.

VII. POTTS-TYPE VICSEK MODEL ON SQUARE LATTICE

This section considers a two-dimensional Potts-type Vicsek model on a square lattice. Each particle is assumed to move to the neighboring eight sites in this model. Figure III.12(a) shows the eight moving directions $\theta = 2\pi \cdot k/8$ ($k = 0, 1, \cdots, 7$). Particles move in one of the eight directions. The stochastic majority rule determines the moving direction. It is similar to the result of the triangular lattice. We can consider a variety of rules to change the moving direction. Here, we show some numerical results only for one updating rule, although similar results were obtained for other cases. That is, the particles are assumed to move along the direction $\theta_{i,j,t+1}$ with probability $p_g = e^g/(e^g + e^{-g})$, where $\theta_{i,j,t+1}$ is the majority direction at site (i, j), to the direction $\theta_{i,j,t+1} \pm \pi/4$ with probability $(1/3)(1 - p_g)$, and $\theta_{i,j,t+1} \pm \pi/2$ with probability $(1/6)(1 - p_g)$. The periodic boundary conditions are imposed.

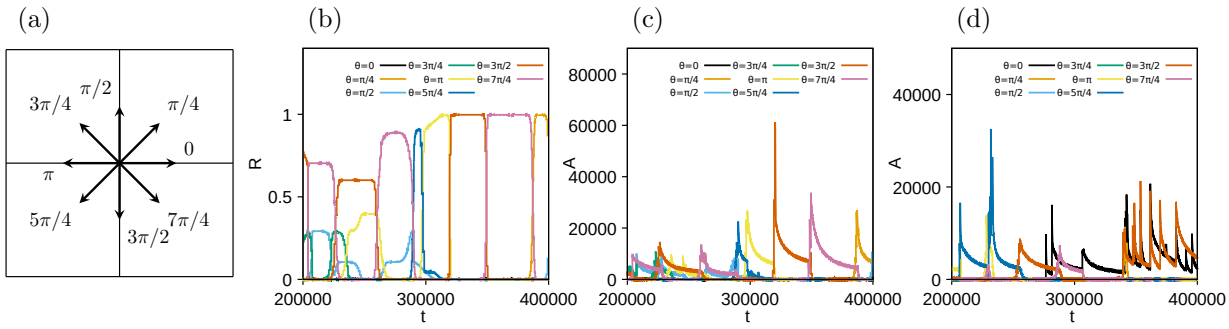

FIG. III.12: (a) Sketch of a particle moving in one of eight directions. (b) Time evolutions of the particle number ratio $R = \sum_{i,j} n^k_{i,j,t}/N$ with the eight moving directions. (c) Maximum value A of $n^k_{i,j,t}$ for the eight moving directions at $L_x \times L_y = 1000 \times 1000$, $N = 4 \times 10^6$, $g = 3$. (d) Maximum value A at $L_x \times L_y = 1000 \times 618 \simeq 1000 \times 1000 \cdot (\sqrt{5}-1)/2$, $N = 2472 \times 10^3 \simeq 4 \times 10^6 \cdot (\sqrt{5}-1)/2$, $g = 3$.

Figure III.12(b) shows the time evolutions of the particle number ratios $\sum_{i,j} n^k_{i,j,t}/N$ for the eight moving directions at $g = 3$. We have performed a numerical simulation of a larger system with $L_x \times L_y = 1000 \times 1000$ and a total particle number of $N = 4 \times 10^6$. Figure III.12(c) shows the maximum value of $n^k_{i,j,t}$ with respect to the lattice points for the eight moving directions. The peak value takes a huge value just after changing the moving direction. Figure III.12(d) shows the result similar to Fig. III.12(c) in a system of $L_x \times L_y = 1000 \times 618 \simeq 1000 \times 1000 \cdot (\sqrt{5}-1)/2$. The direction change repeats even in rectangular lattices of $L_x \neq L_y$.

Figure III.13 shows the directional change of the solitary wave from $t = 318320$. It is observed that $n^k_{i,j,t}$ is strongly localized. Figures III.13(a) and (b) shows the small number of particles moving toward $\theta = 3\pi/2$ (vermillion) and the part of the giant wave moving toward $\theta = \pi$ (yellow). It shows the scene just before the first collision of the two waves. The wave is significantly smaller in radius than the giant wave. Figure III.13(c) shows the scene just after the first collision of the two waves. The small wave collides from the side against the direction of the giant wave. The amplitude and radius of the wave moving toward $\theta = 3\pi/2$ are larger than those before the collision. Figure III.13(d) shows the scene after the first collision of the two waves. Figure III.13(e) shows the scene just before the second collision of the two waves. Figure III.13(f) shows the scene just after the second collision of the two

waves. Then, the size of the wave moving toward $\theta = 3\pi/2$ is significantly larger than that of the wave moving toward $\theta = \pi$. Figure III.13(g) shows the scene just before the third collision of the two waves. Figure III.13(h) shows the scene just after the third collision of the two waves. It shows that the trimodal wave moves toward $\theta = 3\pi/2$. The solitary wave of large amplitude has a trimodal structure just after the three collision processes because it is not a head-on collision. The trimodal wave decays over time. Figure III.13(i) shows it became unimodal, such as the wave moving toward $\theta = \pi$ in Fig. III.13(a). The small wave sweeps up and swallows the main wave over time. The time of the coexistence of the two waves is much shorter than the duration of the one solitary wave. The moving direction changes randomly. However, the moving direction change at each turning process is $\Delta\theta = \pm\pi/4$ or $\pm\pi/2$ in most cases. This is due to the model being set such that a particle of moving direction θ can change its moving direction toward $\theta \pm \pi/4$ or $\theta \pm \pi/2$ with low probabilities.

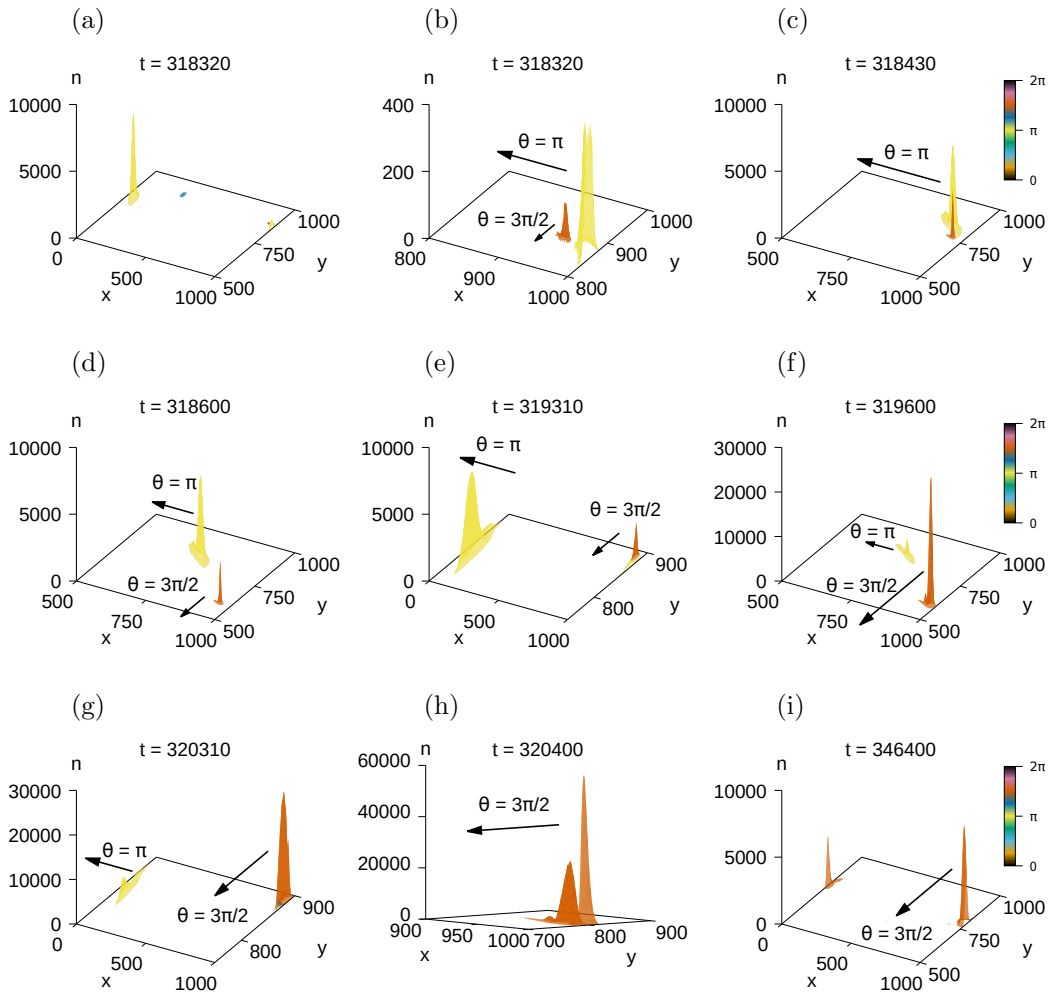

FIG. III.13: Nine snapshot patterns show that a solitary wave changes in the direction of motion from $\theta = \pi$ (yellow) to $\theta = 3\pi/2$ (vermillion) over time. The arrows indicate the direction of motion of the waves. The color bar indicates the direction of the waves. Note that the range of coordinates displayed in the figures is different. Parameters: $L_x \times L_y = 1000 \times 1000$, $N = 4 \times 10^6$, $g = 3$. (a) Solitary wave at $t = 318320$. (b) The enlarged view of (a). Two waves before the first collision. (c) Two waves just after the first collision at $t = 318430$. (d) Two waves after the first collision at $t = 318600$. (e) Two waves before the second collision at $t = 319310$. (f) Two waves after the second collision at $t = 319600$. (g) Two waves before the third collision at $t = 320310$. (h) Single wave after the third collision at $t = 320400$. The wave has trimodal humps. The magnification rate and perspective are different for (a)–(g). (i) Solitary wave at $t = 346400$. The trimodal wave at $t = 320400$ becomes unimodal over time.

VIII. SUMMARY

We proposed the Ising-type Vicsek and Potts-type Vicsek models, exhibiting the collective change in moving direction. The direction of motion of particles in the Ising-type Vicsek Model can take one of two states: the right or left. The direction of motion of particles in the Potts-type Vicsek Model can take one of three or more arbitrary l states: $2\pi/l, 2\pi/(l-1), \cdots, 2\pi/(l-l-1)$. Also, in the Vicsek model, self-propelled particles interact with particles in the neighboring lattice points. We have found that flip motion and directional changes of solitary wave redirection occur in one and two dimensions. The spatially uniform ordered state is stable when the number fluctuations are neglected. We have found that the flip motion occurs with the nucleation of a small population moving in a direction different from the majority group and the subsequent sweeping-up process. The nucleation of a small population moving in another direction occurs with the stochasticity in the updating rule; the majority rule causes the sweeping-up process. The minority changes into the majority after the sweeping-up process. Strongly localized states appear after the rapid direction change of collective motion. In other words, the solitary wave state is maintained by the stochastic direction changes in our model. On the other hand, the spatially uniform state is unstable in the motility-induced phase separation; the cluster generated by the motility-induced phase separation is moving with a steady velocity and has a stationary structure such as the band structure. The formation mechanism of the solitary wave state in our model is different from the motility-induced phase separation seen in the AIM and APM.

Chapter Ⅳ

General conclusion

Ⅰ. CONCLUSION AND FUTURE PROSPECTS

We concentrated on solitary wave formation in this paper in Chapter Ⅱ. We have found that the solitary wave state appears naturally in the direct numerical simulation of the nonlinear Kramers equation, similar to the Vicsek model. One of the differences is that the Vicsek model interacts with particles in the neighborhood. However, our model interacts with all particles, although the interaction with distant particles is small due to Gaussian functions in the integral term. A change in the formation of the solitary wave state may appear when our model interacts only with particles in the neighborhood.

We concentrated on the stochastic directional change that maintains the solitary wave state in this paper in Chapter Ⅲ. Most rectangle band structures move in the short axis direction. However, Refs. [39, 40] reported a numerical model that the direction of motion of the band changed depending on a parameter. The direction of motion takes either the long or the short axis direction. Besides, Ref. [26] reported a mathematical model describing snake-like moving clusters and traveling bands. The study of novel pattern dynamics may reveal the mechanisms of the complex collective motion of living things and the relationship to various states.

In our models, the minority sometimes wins over the majority by local majority rule like a majority of the minority used blocking corporate takeovers. When the majority of the minority is used, only shareholders, excluding major shareholders and shareholders with common interests, can vote. In reality, the opinions of the minority are sometimes more respected than those of the majority. Sometimes the options of the minority are ultimately better than those of the majority. Our model might be applied to a simple model for opinion dynamics.

Galam has applied the Ising model to sociophysics [46]. The model and derivative model have been studied in opinion dynamics [47–49]. Depending on individual models, individual agents can interact with randomly selected others or interact within a short distance space.

Agents have different characteristics: some follow majority rule and have passionate opinions. The particles in our models all have the same properties. Our model, which is simple for individual natures, might bring a new perspective to opinion dynamics.

The positions of the particles in the Ising-type Vicsek model and the Potts-type Vicsek model will be updated simultaneously. We have not considered the update rules for those models, but Ref. [50] reported that different update rules could make differences in the formation of collective motion. Conventional cellular automata use synchronous updates, but various asynchronous updates have been used [51]. Comparing Ising-type and Potts-type Vicsek models with simultaneous and asynchronous updates may improve our understanding of the impact of interactions on collective motion.

The formation mechanism of the solitary wave state in our model is different from the motility-induced phase separation as seen in the active Ising model (AIM) and the active Potts model (APM). There is no velocity difference between the particles since particles in our models have a constant speed in this paper (e.g., velocities in Ising-type Vicsek model takes -1 or 1). Suppose our model incorporates elements with velocities of -1, 0, and 1, or with reduced velocities at high densities. In that case, it might clarify the relationship between our models and AIM and APM models in detail.

Acknowledgments

I would like to thank Associate Professor Hidetsugu Sakaguchi with the Faculty of Engineering Sciences, Kyushu University. He is my Supervisor and Thesis Reviewer for my doctoral dissertation. He often corrected my course when I took a wrong turn in my doctoral program. Without his support, I wouldn't be what I am today.

I would like to thank Professor Tsuyoshi Yoshitake with the Faculty of Engineering Sciences, Kyushu University. He is Chief Thesis Reviewer for my doctoral dissertation. He provided me with meaningful discussions and advice to improve my thesis.

I would like to thank Professor Tohru Hada with the Faculty of Engineering Sciences, Kyushu University. He is Thesis Reviewer for my doctoral dissertation. He provided me with meaningful discussions and advice to improve my thesis.

I would like to thank Professors, Secretaries, Colleagues, CA-Staffs, FIT-Staffs, FU-Staffs, GA-Staffs, IGSES-Staffs, KU-Staffs, Sonne-Staffs, Friends, Neighborhood, my Family, and Relatives for their kind support.

References

[1] T. Vicsek, A. Czirók, E. Ben-Jacob, I. Cohen, and O. Shochet, Phys. Rev. Lett. **75**, 1226 (1995).

[2] T. Vicsek and A. Zafeiris, Phys. Rep. **517**, 71 (2012).

[3] A. Sokolov, I. S. Aranson, J. O. Kessler, and R. E. Goldstein, Phys. Rev. Lett. **98**, 158102 (2007).

[4] V. Schaller, C. Weber, C. Semmrich, E. Frey, and A. R. Bausch, Nature (London) **467**, 73 (2010).

[5] Y. Katz, K. Tunstrøm, C. C. Ioannou, C. Huepe, and I. D. Couzin, Proc. Natl. Acad. Sci. U.S.A. **108**, 18720 (2011).

[6] S. Thutupalli, R. Seemann, and S. Herminghaus, New J. Phys. **13**, 073021 (2011).

[7] Y. Sumino, K. H. Nagai, Y. Shitaka, D. Tanaka, K. Yoshikawa, H. Chaté, and K. Oiwa, Nature (London) **483**, 448 (2012).

[8] T. Ohta, J. Phys. Soc. Jpn. **86**, 072001 (2017).

[9] J. Toner and Y. Tu, Phys. Rev. Lett. **75**, 4326 (1995).

[10] M. C. Marchetti, J. F. Joanny, S. Ramaswamy, T. B. Liverpool, J. Prost, M. Rao, and R. A. Simha, Rev. Mod. Phys. **85**, 1143 (2013).

[11] G. Grégoire and H. Chaté, Phys. Rev. Lett. **92**, 025702 (2004).

[12] N. Shimoyama, K. Sugawara, T. Mizuguchi, Y. Hayakawa, and M. Sano, Phys. Rev. Lett. **76**, 3870 (1996).

[13] H. Chaté, F. Ginelli, G. Grégoire, F. Peruani, and F. Raynaud, Eur. Phys. J. B **64**, 451 (2008).

[14] E. Bertin, M. Droz, and G. Grégoire, Phys. Rev. E **74**, 022101 (2006).; J. Phys. A **42**, 445001 (2009).

[15] S. Mishra, A. Baskaran, and M. C. Marchetti, Phys. Rev. E **81**, 061916 (2010).

[16] A. Gopinath, M. F. Hagan, M. C. Marchetti, and A. Baskaran, Phys. Rev. E **85**, 061903 (2012).

[17] T. Ihle, Phys. Rev. E **88**, 040303(R) (2013).

[18] O. Thual and S. Fauve, J. Phys. (Paris) **49**, 1829 (1988).

[19] H. Sakaguchi, Prog. Theor. Phys. **87**, 1409 (1992).

[20] K. Krischer and A. Mikhailov, Phys. Rev. Lett. **73**, 3165 (1994).

[21] O. Descalzi, J. Cisternas, D. Escaff, and H. R. Brand, Phys. Rev. Lett. **102**, 188302 (2009).

[22] A. Bricard, J. B. Caussin, N. Desreumaux, O. Dauchot, and D. Bartolo, Nature (London) **503**, 95 (2013).

[23] H. Kuwayama, and S. Ishida, Sci. Rep. **3**, 2272 (2013).

[24] S. Yamanaka and T. Ohta, Phys. Rev. E **89**, 012918 (2014).

[25] M. Hayakawa, T. Hiraiwa, Y. Wada, H. Kuwayama, and T. Shibata, eLife **9**, e53609 (2020).

[26] T. Hiraiwa, Phys. Rev. Lett. **125**, 268104 (2020).

[27] J. B. Caussin, A. Solon, A. Peshkov, H. Chaté, T. Dauxois, J. Tailleur, V. Vitelli, and D. Bartolo, Phys. Rev. Lett. **112**, 148102 (2014).

[28] Y. Kuramoto and D. Battogtokh, Nonlinear Phenomena in Complex Systems (Dordrecht, Neth.) **5**, 380 (2002).

[29] Y. Kuramoto, *Chemical Oscillation, Waves, and Turbulence* (Springer-Verlag, Berlin, 1984).

[30] H. Sakaguchi, Phys. Rev. E **70**, 022901 (2004).

[31] H. Sakaguchi and K. Ishibashi, J. Phys. Soc. Jpn. **86**, 114003 (2017).

[32] H. Sakaguchi and K. Ishibashi, J. Phys. Soc. Jpn. **87**, 064001 (2018).

[33] R. Hayakawa, K. Ito, Y. Kimura, and K. Okano, *Introduction to the dynamics of non-equilibrium systems* (Baifukan, Japan, 2006) [published in Japanese].

[34] A. P. Solon and J. Tailleur, Phys. Rev. Lett. **111**, 078101 (2013).

[35] A. P. Solon and J. Tailleur, Phys. Rev. E **92**, 042119 (2015).

[36] A. P. Solon, H. Chaté, and J. Tailleur, Phys. Rev. Lett. **114**, 068101 (2015).

[37] J. Tailleur and M. Cates, Phys. Rev. Lett. **100**, 218103 (2008).

[38] M. Cates and J. Tailleur, Annu. Rev. Condens. Matter Phys. **6**, 219 (2015).

[39] S. Chatterjee, M. Mangeat, R. Paul, and H. Rieger, Europhys. Lett. **130**, 66001 (2020).

[40] M. Mangeat, S. Chatterjee, R. Paul, and H. Rieger, Phys. Rev. E **102**, 042601 (2020).

[41] M. Ballerini, N. Cabibbo, R. Candelier, A. Cavagna, E. Cisbani, I. Giardina, A. Orlandi, G. Parigi, A. Procaccini, M. Voale, and V. Zdravkovic, Anim. Behav. **76**, 201 (2008).

[42] H. Ebata and M. Sano, Sci. Rep. **5**, 8546 (2015).

[43] M. Tamara and T. Ohta, Europhys. Lett. **114**, 30002 (2016).

[44] S. Tanaka, S. Nakata, and M. Nagayama, Soft Matter **17**, 388 (2021).

[45] H. Sakaguchi and K. Ishibashi, Phys. Rev. E **100**, 052113 (2019).

[46] S. Galam, Physica A **238**, 66 (1997).

[47] S. Galam, Physica A **274**, 132 (1999).

[48] R. Hegselmann, and U. Krause, J. Artif. Soc. Soc. Simul. **5**, 3, 2 (2002).

[49] M. Tiwari, X. Yang, and S. Sen, Physica A **582**, 126287 (2021).

[50] D. Strömbom, T. Hassan, W. H. Greis and A. Antia, R. Soc. open sci. **6**, 190381 (2019).

[51] N. Fatès, J. Cellular Automata, **9**, 5–6, 387–416 (2014).